Physics of Fluids

RESEARCH ARTICLE | FEBRUARY 06 2024

Thermodynamic analysis of anomalous region, critical point, and transition from subcritical to supercritical states: Application to van der Waals and five real fluids

Guo-Xiang Wang (王国祥) ; Laura M. Almara ; Vish Prasad (विश प्रसाद)

Physics of Fluids 36, 026105 (2024)
https://doi.org/10.1063/5.0179651

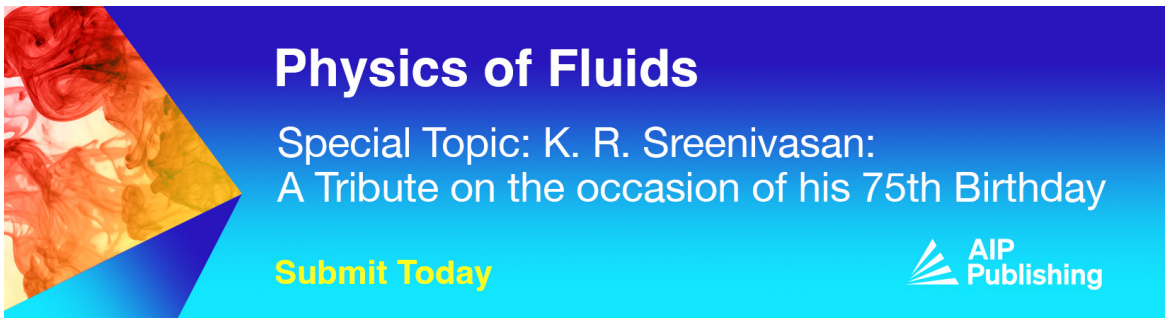

Physics of Fluids ARTICLE pubs.aip.org/aip/pof

Thermodynamic analysis of anomalous region, critical point, and transition from subcritical to supercritical states: Application to van der Waals and five real fluids

Cite as: Phys. Fluids **36**, 026105 (2024); doi: 10.1063/5.0179651
Submitted: 3 October 2023 · Accepted: 1 January 2024 ·
Published Online: 6 February 2024

Guo-Xiang Wang (王国祥),[1] Laura M. Almara,[2] and Vish Prasad (विश प्रसाद)[2,a)]

AFFILIATIONS

[1]Department of Mechanical Engineering, The University of Akron, Akron, Ohio 44325, USA
[2]Department of Mechanical Engineering, University of North Texas, UNT Discovery Park, Denton, Texas 76207, USA

[a)]Author to whom correspondence should be addressed: vish.prasad@unt.edu

ABSTRACT

All fluids exhibit large property-variations near the critical point in a region identified as the anomalous state. The anomaly starts in the liquid and extends well into the supercritical state, which can be identified thermodynamically using the Gibbs free energy (g). The specific heat, isobaric expansion, and isothermal compressibility parameters governing the transitions are: (c_p/T), $(v\beta)$, and $(v\kappa)$, rather c_p, β, and κ. They are essentially the second-order derivatives of g and have two extrema (minimum, maximum); only maxima reported ever. When applied to the van der Waals fluid, these extrema exhibit closed loops on the phase-diagram to satisfy $d^3g = 0$ and map the anomalous region. The predicted liquid-like to gas-like transitions are related to the ridges reported earlier, and the Widom delta falls between these loops. Evidently, in the anomalous region, both the liquid and the supercritical fluid need to be treated differently. Beyond the anomalous states, the supercritical fluids show monotonic, gradual changes in their properties. The analysis for argon, methane, nitrogen, carbon dioxide, and water validates the thermodynamic model, supports the stated observations, and identifies their delimiting pressures and temperatures for the anomalous states. It also demonstrates the applicability of the law of corresponding states. Notably, the critical point is a state where $d^3g = 0$, the anomaly in the fluid's properties/behavior is maximal, and the governing parameters approach infinity. Also the following are presented: (a) the trajectory of the liquid–vapor line toward the melt-solid boundary and (b) a modified phase diagram (for water) exhibiting the anomalous region.

I. INTRODUCTION

All fluids exhibit large-scale property variations near the critical point (CP). For example, the density, dynamic viscosity, and thermal conductivity drop sharply near the CP whereas the specific heat first increases with temperature, achieves a peak, and then decreases to a monotonic behavior, the peak being highest at the CP. Ultimately, the properties revert to monotonic behavior at high SC pressures and temperatures. This anomalous behavior in the SC region close to CP, also referred to as the pseudo-critical region,[1] may offer advantages in some applications but is highly complex. Indeed, as the applications of supercritical fluids expand in turbulent flow systems,[2,3] nano-channels,[4] heat and mass transfer,[5,6] thermal power plants,[7] energy systems,[8] atomization and jets,[9] mixing and extraction,[10] supersonic shocks,[11] carbon capture and storage,[12] and so on, the understanding of fluids moving from the subcritical to supercritical state via the anomalous region becomes extremely important.

In a series of papers published in 1997–2004,[13–16] Nishikawa and co-workers have emphasized that inhomogeneity is the most fundamental concept of the states of SC fluids, and the density fluctuation as a measure of this inhomogeneity is one of the fundamental parameters that determine their physico-chemical properties. They have shown that when the contour map of specific maximum of isothermal changes in density fluctuations of van der Waals (vdW) fluid is drawn on its phase diagram, there exists a ridge, referred to as the Nishikawa ridge.[15] The ridge separates the SC region in two parts and is the locus of the points where the third derivatives of the Gibbs free energy become zero. Their results also demonstrate the extension of the ridge to the subcritical region.

Later, Sato *et al.*[17] observed that the ridge can be interpreted as the boundary by which the supercritical state is divided into "liquid-like" (SCLL) and "gas-like" (SCGL) states. Evidently, the SC fluids do not have a homogenous phase as thought previously. Instead, it can be roughly divided into two states, and there is a transition from the liquid-like to gas-like state as the temperature increases isobarically, or the pressure increases isothermally. Many attempts have been made to identify such transitions on the *P-T* and *T-v* phase diagrams.

Xu *et al.*[18] investigating a two-water model found a correlation between the dynamic crossover and the locus of the specific heat maxima and called it the "Widom line." They believed that locations of maxima of different SC properties may not lie far from each other, and one line may be sufficient to determine the crossover from the SCLL to SCGL behavior; the Widom line based on $c_{p,max}$ has also been referred to as the pseudo-critical line.[1] The data presented by Simeoni *et al.*[19] for neon, oxygen, argon, and nitrogen do show liquid-like and gas-like regions for the reduced pressure, $P_r > 1$ and temperature, $T_r > 1$.

Surprisingly, Brazhkin *et al.*[20] found that even in the case of simplest Lennard–Jones fluid, the lines for maxima of various properties may lie away from each other, as also shown by other authors. These properties may include density; isobaric, isochoric, and isentropic specific heats; isothermal and isentropic compressibility; coefficient of volumetric expansion; speed of sound; and transport properties such as thermal conductivity, viscosity, and mass diffusivity. Indeed, the lines of maxima diverge significantly in a *P-T* plane,[21–24] but the ridge for specific heat approaches close to the critical isochore.[21] This raises the question, do we need to consider all of these properties to prescribe the behavior of a SC fluid in the anomalous region?

Recently, Banuti *et al.*,[25] through an extensive thermodynamic analysis, molecular dynamics (MD) simulation, and experiments, have proposed a new interpretation of the Widom line based on the curvature of the Gibbs free energy. They have argued that the SC crossover can be evaluated as a projection of the subcritical phase transition from liquid to vapor. Their results demonstrate that the crossover from SCLL to SCGL across the Widom line is not instantaneous but over a finite temperature interval; referred to as the Widom Delta[26,27] or transitional region associated with the pool boiling.[25,28] They have shown that thermodynamically the importance of the Widom line goes down at $P_r \approx 3$ and disappears at $P_r \approx 10$. Some authors, including Banuti,[28] have argued that there is a supercritical analog to the subcritical phase-change when crossing the line of demarcation, and named it pseudo-boiling. It occurs in the phase equilibrium over a finite temperature interval. An excellent review of the literature on transitions in the SC states of matter, including experimental evidence, has been presented recently by Cockrell *et al.*[29]

Surprisingly, most of the above works and their discussions focus on the conditions beyond the critical point, except the works of Nishikawa *et al.*,[15] Brazhkin *et al.*,[24] Banuti *et al.*,[25] and a few others who have mentioned the ridges in the subcritical phase. Indeed, the anomalous behavior, that is characterized by large-scale changes in fluid properties and even reversal, continues to exist below the critical pressure and/or the critical temperature. As argued recently by Prasad *et al.*,[23] the subcritical liquid should also be divided into two states: (a) one the "regular liquid" as we know and (b) the other where the liquid properties are anomalous and may exhibit similar behavior as the SCLL. Apparently, the second state of the subcritical liquid and the first state of the SC fluid (liquid-like) ought to be continuous.[23] A similar concept of two states of liquid as "Rigid" and "Non-rigid" was presented by Brazhkin *et al.*[24] in the supercritical region, also see Ref. 29. Referring to the second state of subcritical liquid as the non-rigid liquid may be justified since the density drops significantly even in the region below P_c and T_c (evident from the plots using REFPROP[30]).

Prasad *et al.*[23] have shown schematically (Fig. 1) the anomalous region bounded by PLQ and PGQ. It consists of the non-rigid liquid and vapor in the subcritical region, and the SCLL and SCGL states in the supercritical region. The SCGL state ends at the line PGQ, beyond which (on the right) the SC state with no large-scale variations and inversions in thermophysical properties would exist. Similarly, on the subcritical side, the gas would not exhibit any anomalous behavior on the right of PGQ. Note that on a traditional phase-diagram, point P is directly connected to CP through the liquid-vapor phase change line (black solid line in Fig. 1). However, the shape and extent of anomalous region (between PLQ and PGQ) may vary based on the fluid and

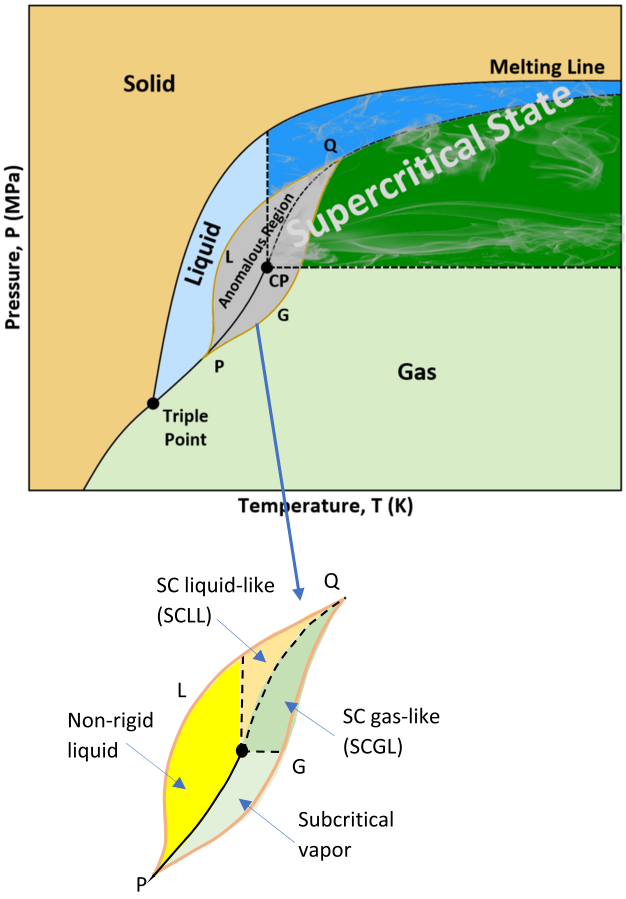

FIG. 1. Schematic of the phase-diagram depicting the anomalous state, which consists of the non-rigid liquid and vapor phases in the subcritical region and the liquid-like and gas-like states in the supercritical region; the shape and extent of this region may depend on the fluid and its properties. Modified Fig. 6, with permission from Prasad *et al.*,[23] "Existence of supercritical 'liquid-like' state in subcritical region, optimal heat transfer enhancement, and argon as a non-reacting, non-corroding SC heat transfer fluid," Heat Transfer Res. **53**(9), 1–27 (2022). Copyright 2022 Begell House, Inc.

its properties. Evidently, on the left of line PLQ, the fluid is in the (rigid) liquid state.

We present here a unified thermodynamic analysis of the entire anomalous region by examining the variations in thermodynamic properties from the subcritical to supercritical states. Note that in the SC region, this model is restricted to the states dominated by thermodynamics rather than by the dynamics.[31] We follow the Gibbs free energy approach as proposed by Nishikawa *et al.*[15] in 2003. The analysis reveals that it is the modified thermodynamic parameters, (c_p/T), $(v\beta)$, and $(v\kappa)$, that need to be considered instead of c_p, β, and κ, to analyze the thermodynamic phase transitions and study the behavior of the anomalous states. They are essentially the second-order derivatives of the Gibbs free energy. Banuti *et al.*[25] have obtained the thermodynamic response function, $c_p/T = -(d^2g/dT^2)_p$ based on the curvature of Gibbs surface to identify the distinct liquid-like and gas-like regions, divided by a crossover line.

In this paper, we introduce six third-order derivatives of Gibbs free energy and equate them to zero $(d^3g = 0)$[15,16] to identify the loci of extrema that can map the anomalous region in both the subcritical and supercritical regions. A detailed analysis is carried out by using the simple van der Waals (vdW) fluid and then applied to five real fluids: argon, methane, nitrogen, carbon dioxide, and water. The analysis also leads to an expanded definition of the critical point. Finally, the importance of the delimitation of anomalous region is discussed, and an important practical application is presented.

II. THERMODYNAMIC ANALYSIS BASED ON GIBBS FREE ENERGY

For a pure substance, the Gibbs free energy, $g(T, P)$ can be written as

$$g = h - Ts = u + Pv - Ts. \tag{1}$$

Differentiation of which leads to

$$dg = \left(\frac{\partial g}{\partial T}\right)_P dT + \left(\frac{\partial g}{\partial P}\right)_T dP = -sdT + vdP, \tag{2}$$

$$d^2g = \left(\frac{\partial^2 g}{\partial T^2}\right)_P dT^2 + 2\left(\frac{\partial^2 g}{\partial T \partial P}\right) dTdP + \left(\frac{\partial^2 g}{\partial P^2}\right)_T dP^2, \tag{3}$$

$$d^3g = \left(\frac{\partial^3 g}{\partial T^3}\right)_P dT^3 + 3\left(\frac{\partial^3 g}{\partial T^2 \partial P}\right) dT^2 dP + 3\left(\frac{\partial^3 g}{\partial T \partial P^2}\right) dTdP^2 + \left(\frac{\partial^3 g}{\partial P^3}\right)_T dP^3. \tag{4}$$

Using

$$\left(\frac{\partial g}{\partial T}\right)_P = -s \quad \text{and} \quad \left(\frac{\partial g}{\partial P}\right)_T = v, \tag{5}$$

we obtain[32]

$$\textit{Isobaric specific heat},\ c_p = \left(\frac{\partial h}{\partial T}\right)_P = T\left(\frac{\partial s}{\partial T}\right)_P = T\left[\frac{\partial}{\partial T}\left(-\frac{\partial g}{\partial T}\right)_P\right]_P = -T\left(\frac{\partial^2 g}{\partial T^2}\right)_p, \tag{6}$$

$$\textit{Isobaric coefficient of expansion},\ \beta = \frac{1}{v}\left(\frac{\partial v}{\partial T}\right)_P = \frac{1}{v}\left[\frac{\partial}{\partial T}\left(\frac{\partial g}{\partial P}\right)_T\right]_P = \frac{1}{v}\left(\frac{\partial^2 g}{\partial T \partial P}\right), \tag{7}$$

$$\textit{Isothermal compressibility},\ \kappa = -\frac{1}{v}\left(\frac{\partial v}{\partial P}\right)_T = -\frac{1}{v}\left[\frac{\partial}{\partial P}\left(\frac{\partial g}{\partial P}\right)_T\right]_T = -\frac{1}{v}\left(\frac{\partial^2 g}{\partial P^2}\right)_T \tag{8}$$

that leads to the three thermodynamic parameters, as follows:

$$\textit{Isobaric specific heatparameter},\ -\left(\frac{\partial^2 g}{\partial T^2}\right)_p = \frac{c_P}{T}, \tag{9a}$$

$$\textit{Isobaric volumetric expansion parameter},\ \left(\frac{\partial^2 g}{\partial T \partial P}\right) = v\beta, \tag{9b}$$

$$\text{and, } \textit{Isothermal compressibility parameter},\ -\left(\frac{\partial^2 g}{\partial P^2}\right)_T = v\kappa. \tag{9c}$$

Note that Banuti *et al.*[25] had introduced Eq. (9a) earlier.
Substituting them into Eq. (3) yields

$$d^2g = -\frac{c_P}{T}dT^2 + 2v\beta dTdP - v\kappa dP^2. \tag{10}$$

Correspondingly, the third-order derivatives of the Gibbs free energy are related to the first-order derivatives of the above parameters [Eq. (9)]

$$\left(\frac{\partial^3 g}{\partial T^3}\right)_p = \frac{\partial}{\partial T}\left(\frac{\partial^2 g}{\partial T^2}\right)_p = -\left[\frac{\partial}{\partial T}\left(\frac{c_P}{T}\right)\right]_P = \zeta_1, \tag{11}$$

$$\left(\frac{\partial^3 g}{\partial P \partial T^2}\right) = \left[\frac{\partial}{\partial P}\left(\frac{\partial^2 g}{\partial T^2}\right)_P\right]_T = -\left[\frac{\partial}{\partial P}\left(\frac{c_P}{T}\right)\right]_T = \zeta_{2,T}, \tag{12a}$$

$$\left(\frac{\partial^3 g}{\partial T^2 \partial P}\right) = \left[\frac{\partial}{\partial T}\left(\frac{\partial^2 g}{\partial T \partial P}\right)\right]_P = \left[\frac{\partial(v\beta)}{\partial T}\right]_P = \zeta_{2,P}, \tag{12b}$$

$$\left(\frac{\partial^3 g}{\partial P \partial T \partial P}\right) = \left[\frac{\partial}{\partial P}\left(\frac{\partial^2 g}{\partial T \partial P}\right)\right]_T = \left[\frac{\partial(v\beta)}{\partial P}\right]_T = \zeta_{3,T}, \tag{13a}$$

$$\left(\frac{\partial^3 g}{\partial T \partial P^2}\right) = \left[\frac{\partial}{\partial T}\left(\frac{\partial^2 g}{\partial P^2}\right)_T\right]_P = -\left[\frac{\partial(v\kappa)}{\partial T}\right]_P = \zeta_{3,P}, \tag{13b}$$

$$\left(\frac{\partial^3 g}{\partial P^3}\right)_T = \frac{\partial}{\partial P}\left(\frac{\partial^2 g}{\partial P^2}\right)_T = -\left[\frac{\partial(v\kappa)}{\partial P}\right]_T = \zeta_4. \tag{14}$$

In Eqs. (11)–(14), we have introduced six parameters, ζ_i with $i = 1$, 2, 3, and 4, to represent the corresponding third-order derivatives of g with respect to T and P.

In the case of cross-derivatives, Eqs. (12) and (13), a second subscript, P or T, is used to denote the isobaric or isothermal process, respectively. If the function g is continuous in the third-order, as assumed in Eq. (3) also, we can write

$$\zeta_{2,T} = z_{2,P} = \zeta_2, \text{ and } \zeta_{3,T} = \zeta_{3,P} = \zeta_3. \tag{15}$$

In that case, the negative isothermal derivative of (c_p/T) with respect to P is equal to the isobaric derivative of $(v\beta)$ with T [Eqs. (12a) and (12b)]. Similarly, the isothermal derivative of $(v\beta)$ with respect to P is equal to the isobaric derivative of $(v\kappa)$ with T [Eqs. (13a) and (13b)]. Although switching the order of differentiation may not be valid at the critical as well as the liquid-vapor points, Eq. (15) should be applicable to all other (P, T) states as shown by the equation of state (EOS) for vdW fluid in Sec. III A. Substituting Eqs. (11)–(15) in Eq. (4) leads to

$$d^3g = \zeta_1 dT^3 + 3\zeta_2 dT^2 dP + 3\zeta_3 dT dP^2 + \zeta_4 dP^3. \tag{16}$$

Following Refs. 15 and 16, the anomalous behavior and ridges of the thermodynamic properties should be related to the consequences of $d^3g = 0$, which needs to satisfy the following four conditions:

$$\zeta_1 = \left[\frac{\partial}{\partial T}\left(\frac{c_P}{T}\right)\right]_P = 0, \tag{17a}$$

$$\zeta_2 = \left[\frac{\partial}{\partial P}\left(\frac{c_P}{T}\right)\right]_T = \left[\frac{\partial(v\beta)}{\partial T}\right]_P = 0, \tag{17b}$$

$$\zeta_3 = \left[\frac{\partial(v\beta)}{\partial P}\right]_T = \left[\frac{\partial(v\kappa)}{\partial T}\right]_P = 0, \text{ and} \tag{17c}$$

$$\zeta_4 = \left[\frac{\partial(v\kappa)}{\partial P}\right]_T = 0. \tag{17d}$$

It should be pointed out that zeros of the above four third-order derivatives will lead to the loci of the extrema of three modified thermodynamic parameters, (c_p/T), $(v\beta)$, and $(v\kappa)$. In the literature, however, the Widom lines are the loci of the maxima of the traditional thermodynamic properties c_p, β, κ, and so on.

These conditions [Eqs. (17a)–(17d)] can also be rewritten in terms of the measurable properties, c_p and v as

$$\zeta_1 = \left(\frac{\partial^3 g}{\partial T^3}\right)_P = -\left[\frac{\partial}{\partial T}\left(\frac{c_P}{T}\right)\right]_P = 0, \tag{18a}$$

$$\zeta_2 = \left(\frac{\partial^3 g}{\partial T^2 \partial P}\right) = \left[\frac{\partial(v\beta)}{\partial T}\right]_P = \left[\frac{\partial}{\partial T}\left(\frac{\partial v}{\partial T}\right)_P\right]_P = \left(\frac{\partial^2 v}{\partial T^2}\right)_P = 0, \tag{18b}$$

$$\zeta_3 = \left(\frac{\partial^3 g}{\partial T \partial P^2}\right) = \left[\frac{\partial(v\beta)}{\partial P}\right]_T = \left[\frac{\partial}{\partial P}\left(\frac{\partial v}{\partial T}\right)_P\right]_T = \left(\frac{\partial^2 v}{\partial T \partial P}\right) = 0, \tag{18c}$$

$$\zeta_4 = \left(\frac{\partial^3 g}{\partial P^3}\right)_T = \left[\frac{\partial(v\kappa)}{\partial P}\right]_T = -\left[\frac{\partial}{\partial P}\left(\frac{\partial v}{\partial P}\right)_T\right]_T = -\left(\frac{\partial^2 v}{\partial P^2}\right)_T = 0. \tag{18d}$$

The loci of the extrema of (c_p/T), $(v\beta)$, and $(v\kappa)$, then correspond to the zero values of the first derivative of the parameter, (c_p/T), and the second derivatives of the specific volume, v, with either temperature, or pressure, or both [Eqs. (18a)–(18d)]. Although (c_p/T) has been used by Banuti and co-workers,[28,33] $(v\beta)$ and $(v\kappa)$ have never been considered in the literature.

III. APPLICATION TO THE VAN DER WAALS AND OTHER FLUIDS

A. van der Waals fluid

We first consider the van der Waals (vdW) fluid to apply the above model and seek the loci of $\zeta_i = 0$ on a P-T phase-diagram. The vdW equation of state (EOS) is usually written as[34]

$$P = \frac{RT}{v - b} - \frac{a}{v^2}, \tag{19}$$

where R is the gas constant and a and b are constants, characteristics of the specific fluid. These two constants can be determined by the critical pressure, P_c, temperature, T_c, and specific volume, v_c, with the condition of the zeros of the first and second derivatives of pressure with specific volume along the isotherms

$$a = \frac{9}{8} R T_c v_c \text{ and } b = \frac{v_c}{3}, \tag{20a}$$

which lead to

$$P_c = \frac{a}{27b^2} \text{ and } T_c = \frac{8a}{27Rb}. \tag{20b}$$

Therefore, the corresponding critical compressibility constant (Z_c) of the vdW fluid is

$$Z_c = \frac{P_c v_c}{R T_c} = \frac{3}{8}. \tag{20c}$$

It should be noted that the vdW EOS is a representative example of the mean field theory and would not fit well in places where the fluctuation effects are large such as near the critical point. Some of the predicted characteristics may, therefore, deviate in the case of real fluids.

Using the reduced pressure, P_r, specific volume, v_r, and temperature T_r, as

$$P_r = \frac{P}{P_c}, \quad v_r = \frac{v}{v_c}, \quad T_r = \frac{T}{T_c}. \tag{21}$$

Equation (19) reduces to

$$P_r = \frac{8T_r}{3v_r - 1} - \frac{3}{v_r^2}. \tag{22}$$

The properties, c_p, β, and κ can then be written in the dimensionless reduced form as

$$\frac{c_p}{R} = \frac{3}{2} + \frac{32 Z_c v_r^3 T_r}{12 v_r^3 T_r - 3(3v_r - 1)^2}, \tag{23}$$

$$\beta T_c = \frac{1}{v_r}\left(\frac{\partial v_r}{\partial T_r}\right)_{P_r} = \frac{4v_r^2(3v_r - 1)}{12 T_r v_r^3 - 3(3v_r - 1)^2}, \tag{24}$$

$$\kappa P_c = -\frac{1}{v_r}\left(\frac{\partial v_r}{\partial P_r}\right)_{T_r} = \frac{(3v_r - 1)^2 v_r^2}{24 T_r v_r^3 - 6(3v_r - 1)^2}, \tag{25}$$

For the vdW fluid, the isochoric specific heat, c_v, is given as $3R/2$. Then, the three modified properties [Eqs. (9a)–(9c)] in the dimensionless reduced form are

$$\frac{c_p}{R T_r} = \frac{3}{2 T_r} + \frac{32 Z_c v_r^3}{A}, \tag{26}$$

$$(\nu_r \beta T_c) = \left(\frac{\partial \nu_r}{\partial T_r}\right)_{P_r} = \frac{4\nu_r^3(3\nu_r - 1)}{A}, \tag{27}$$

$$(\nu_r \kappa P_c) = -\left(\frac{\partial \nu_r}{\partial P_r}\right)_{T_r} = -\frac{(3\nu_r - 1)^2 \nu_r^3}{2A}, \tag{28}$$

where A is a function of ν_r and T_r,

$$A = 12\nu_r^3 T_r - 3(3\nu_r - 1)^2. \tag{29}$$

The dimensionless, reduced forms of the four new parameters, ζ_1, ζ_2, ζ_3, and ζ_4 as defined in Eqs. (11)–(15) can be derived as follows:

$$\zeta_{r1} = \frac{T_c^2}{R}|\zeta_1| = \left[\frac{\partial}{\partial T_r}\left(\frac{c_P}{RT_r}\right)\right]_{P_r} = -\frac{3}{2T_r^2} + \frac{96 Z_c \nu_r^2}{A}\left(\frac{\partial \nu_r}{\partial T_r}\right)_{P_r} - \frac{32 Z_c \nu_r^3}{A^2}\left(\frac{\partial A}{\partial T_r}\right)_{P_r}, \tag{30a}$$

$$\zeta_{r2} = \frac{T_c^2}{\nu_c}\zeta_{2,p} = \left[\frac{\partial(\nu_r \beta T_c)}{\partial T_r}\right]_{P_r} = \frac{12\nu_r^2(4\nu_r - 1)}{A}\left(\frac{\partial \nu_r}{\partial T_r}\right)_{P_r} - \frac{4\nu_r^3(3\nu_r - 1)}{A^2}\left(\frac{\partial A}{\partial T_r}\right)_{P_r}, \tag{30b}$$

$$\zeta_{r3} = \frac{T_c P_c}{\nu_c}\zeta_{3,T} = \left[\frac{\partial(\nu_r \beta T_c)}{\partial P_r}\right]_{T_r} = \left(\frac{\partial^2 \nu_r}{\partial T_r \partial P_r}\right) = \frac{12\nu_r^2(4\nu_r - 1)}{A}\left(\frac{\partial \nu_r}{\partial P_r}\right)_{T_r} - \frac{4\nu_r^3(3\nu_r - 1)}{A^2}\left(\frac{\partial A}{\partial P_r}\right)_{T_r}, \tag{30c}$$

$$\zeta_{r4} = \frac{P_c^2}{\nu_c}\zeta_4 = -\left(\frac{\partial(\nu_r \kappa P_c)}{\partial P_r}\right)_{T_r} = \left(\frac{\partial^2 \nu_r}{\partial P_r^2}\right)_{T_r} = -\frac{3\nu_r^2(3\nu_r - 1)(5\nu_r - 1)}{2A}\left(\frac{\partial \nu_r}{\partial P_r}\right)_{T_r} + \frac{(3\nu_r - 1)^2 \nu_r^3}{2A^2}\left(\frac{\partial A}{\partial P_r}\right)_{T_r}, \tag{30d}$$

where the derivatives of A are given by

$$\left(\frac{\partial A}{\partial T_r}\right)_{P_r} = 12\nu_r^3 + \left[36\nu_r^2 T_r - 18(3\nu_r - 1)\right]\left(\frac{\partial \nu_r}{\partial T_r}\right)_{P_r} \tag{31a}$$

and

$$\left(\frac{\partial A}{\partial P_r}\right)_{T_r} = \left[36\nu_r^2 T_r - 18(3\nu_r - 1)\right]\left(\frac{\partial \nu_r}{\partial P_r}\right)_{T_r}. \tag{31b}$$

Note that Eqs. (30a)–(30d) for ζ_{ri} depend on only ν_r and T_r. The first derivatives of ν_r to T_r and P_r are given in Eqs. (27) and (28), respectively. In Eq. (30a), the negative sign of the original definition is dropped.

For the simple vdW EOS, the following analytical expressions can be obtained:

$$\zeta_{r2} = 0 \quad \nu_r = 1, \tag{32}$$

$$\zeta_{r3} = 0 \quad T_r = \frac{(3\nu_r - 1)^2(2\nu_r - 1)}{4\nu_r^4}, \tag{33}$$

$$\zeta_{r4} = 0 \quad T_r = \frac{(3\nu_r - 1)^3}{8\nu_r^4}. \tag{34}$$

In the case of $\zeta_{r1} = 0$, a root-finding scheme needs to be used to locate the reduced temperatures at any given reduced pressure from Eq. (30a).

For a given state (P_r, T_r), one can solve for ν_r from the cubic vdW equation as

$$3P_r\nu_r^3 - (P_r + 8T_r)\nu_r^2 + 9\nu_r - 3 = 0. \tag{35}$$

Note that there exists only one real solution to Eq. (35) in the SC state, $P_r > 1$. However, under the subcritical conditions ($P_r < 1$), there exist three real roots, selection of which depends on the phase of the state. The smallest root is selected for the liquid phase while the largest root is for the vapor phase; the saturation temperature, $T_{r,v}$, for a given pressure, P_r, is known for the vdW fluid.[34] Indeed, it is a liquid phase if $T_r < T_{r,v}$, otherwise it is the vapor phase. Therefore, the three property functions, c_p/T_rR, $\nu_r\beta T_c$, and $\nu_r\kappa P_c$ can be obtained from Eqs. (26)–(28), together with Eqs. (29) and (35).

B. Other fluids

The benefit of vdW EOS being differentiable with respect to the basic thermodynamic properties, P and T, is not readily available in the case of real fluids. Their equations of states are complex and change with the regimes. Many times they are either empirical or based on the empirical parameters, obtained from the experiments. Therefore, we have used REFPROP[30] to calculate (c_p/T), ($v\beta$), and ($v\kappa$). For the required pressure (P) and temperature (T) of a given fluid, the values for c_p are directly read from REFPROP[30] and divided by the corresponding temperatures to obtain c_p/T. For $v\beta$ and $v\kappa$, we use Eqs. (7) and (8), which require the first-order partial derivatives of the specific volume with T and P, respectively. They are obtained directly from the REFPROP[30] at given P and T. The partial derivatives of c_p/T with temperature, i.e., ζ_1 [Eq. (11)], are then calculated and the locations of extrema ($\zeta_1 = 0$) are identified. Similarly, the locations of extrema of other three derivatives, $\zeta_2 = 0$, $\zeta_3 = 0$, and $\zeta_4 = 0$ [Eqs. (18b)–(18d)], can be calculated using the REFPROP,[30] which gives the second-order partial derivatives of specific volume with either temperature, pressure, or both.

Note that the NIST's REFPROP[30] provides the most accurate values of thermophysical properties for a large number of fluids. REFPROP data have either been obtained experimentally or from the correlations based on the experimental data. Whenever an equation of state has been used to calculate the properties in any particular range of pressure and temperature, the EOS has already been validated in this range. Detailed discussions on the accuracy of these data are readily available in the literature, for example, argon,[35] nitrogen,[36] methane,[37] carbon dioxide,[38] and water.[39] In this sense, our results for all five real fluids can be considered as good as that can be obtained directly from the experimental data, as also stated by Gallo *et al.*[40] They have used the NIST's Chemistry WebBook to obtain the experimental data on water (IAPWS-95/IAPS-EOS) to compare their molecular dynamics predictions for the Widom lines and the dynamical crossover.

It is also important to note that the results presented here are independent of the values of the thermophysical properties at (P_c, T_c), whose accuracy is often questioned. What we require for the present analysis to be exact are that (a) the locations of the critical point be precise and (b) the trends of the property curves be accurate. Indeed, since the locations of the critical point of various fluids reported in the literature have been obtained through carefully-designed experiments, their reliability should be acceptable.

IV. RESULTS AND DISCUSSION

First, we examine the variations in three modified parameters, (c_p/RT_r), $(v_r\beta T_c)$, and $(v_r\kappa P_c)$ with P_r and T_r and identify the possible extrema along the curve, for the vdW fluid. In each case, we compare the behavior of the modified parameter with the original property and examine the implications of the modifications. We also examine the variations in the associated third-order parameter, ζ_{ri}, and identify the zero points. The contour map for each modified parameter is then drawn, which shows that the condition of $\zeta_{ri} = 0$ encloses a region of anomalous variation in the corresponding property, except for ζ_{r2}. Subsequently, we consider five real fluids—argon, nitrogen, methane, carbon dioxide, and water, to examine the universality of the trends and phenomena predicted by the vdW fluid [note that (c_p/T_rR), $(v_r\beta T_c)$, and $(v_r\kappa P_c)$ are directly proportional to (c_p/T), $(v\beta)$, and $(v\kappa)$ since P_c, T_c, v_c, and R are all constants for a given fluid].

A. Isobaric specific heat parameter (c_p/RT_r)

First, we consider the variations in the isobaric specific heat parameter, c_p/RT_r, with T_r and P_r, respectively. It is interesting to note that the isobaric variation of c_p with temperature has been extensively studied in the literature, but rarely the isothermal variations. Figure 2(a) for c_p/R and c_p/RT_r for $P_r = 1.5$ reveals that there exist two extrema, one local maximum and the other local minimum for c_p/T_rR (black line), whereas c_p/R (blue line) has only one extremum, the local maximum but not the local minimum. Correspondingly, there exist two locations for $\zeta_{r1} = 0$ [Fig. 2(b)]. Similarly, for a subcritical pressure, $P_r = 0.6$, there exist two extrema rather than one as shown by c_p/R [Fig. 2(c)]. Below the critical point, both curves show a discontinuity at the point where the phase change from the liquid to vapor occurs; this discontinuity is much better exhibited in Fig. 2(d) for ζ_{r1}.

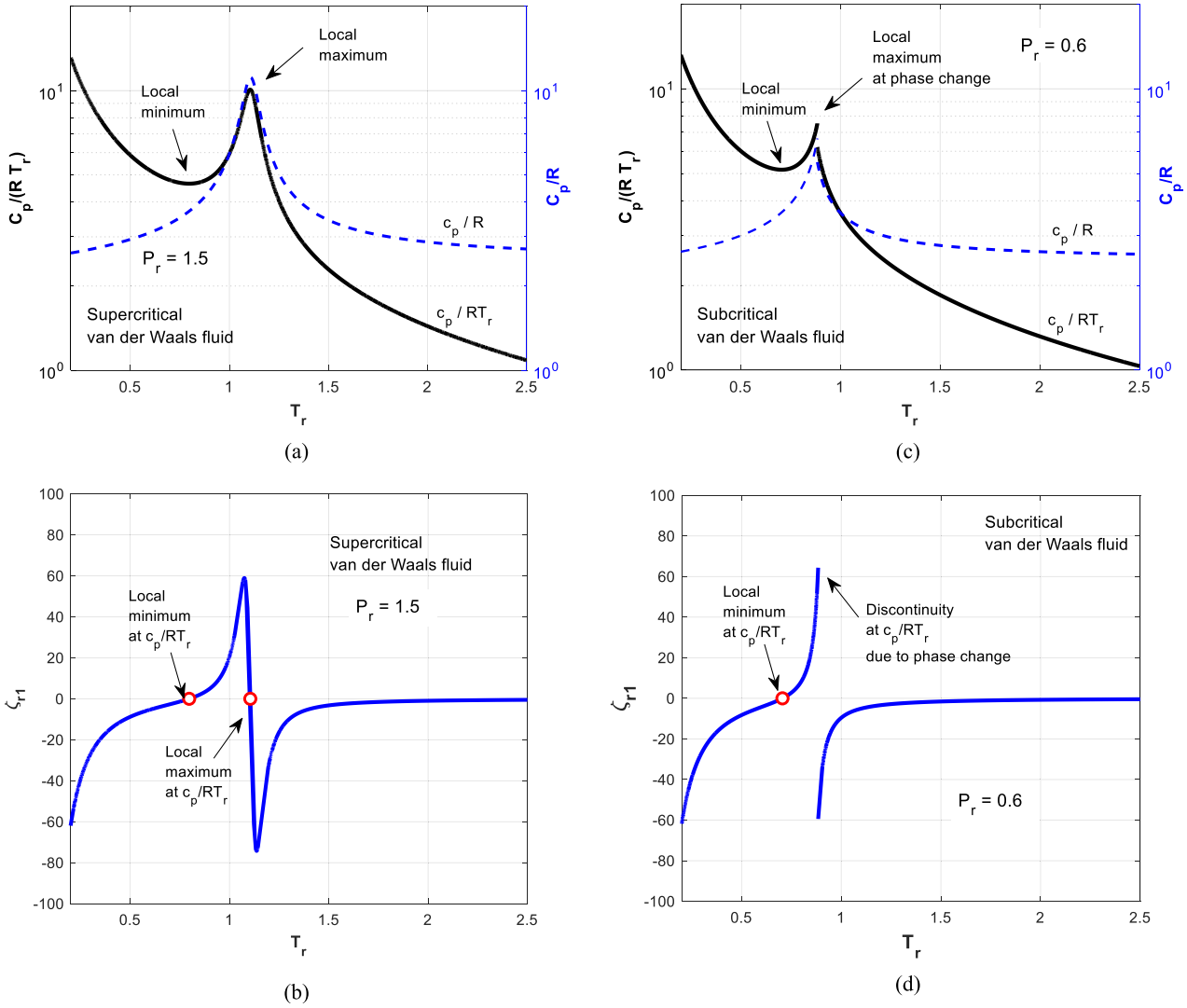

FIG. 2. Variations of (a) c_p/RT_r (black line, left axis) and c_p/R (blue line, right axis), and (b) ζ_{r1} with reduced temperature, T_r at $P_r = 1.5$ of supercritical vdW fluid; (c) c_p/RT_r (black line, left axis) and c_p/R (blue line, right axis) and (d) ζ_{r1} vs reduced temperature, T_r at $P_r = 0.6$ for the subcritical van der Waals fluid.

The above behavior of two extrema of c_p/RT_r is further elaborated in Fig. 3(a) against T_r for a range of reduced pressure, P_r, within the SC state. Again, it is the local maximum that has attracted all attention in the literature, and to our knowledge, the local minimum is being revealed here for the first time. The region bounded by the two extrema, their loci connected by the dashed red line [Fig. 3(a)], shows an inverse change and a ridge, instead of the monotonic behavior on both the inside and outside regions ($T_r \ll 1$ and $T_r \gg 1$). c_p/RT_r inside the region, bounded by the two extrema, continuously increases, which reminds us of the reverse variation of the volume with pressure within the spinodal region. It is, therefore, believed that such a region relates to a thermodynamically important variation. As expected, the peak is highest at the critical point. The local extremum disappears at $P_r \approx 3.227$, beyond which the isobaric curve for c_p/RT_r shows a monotonic behavior from low to high values of T_r [Fig. 3(a)]. This agrees well with the finding of Banuti *et al.*[25]

Evidently, the two extrema of c_p/RT_r in the subcritical state [Fig. 3(b)] support the existence of the anomalous states below the critical point (Fig. 1). As noted earlier, there exists discontinuity of the function at the point of the liquid-vapor phase change, the point of

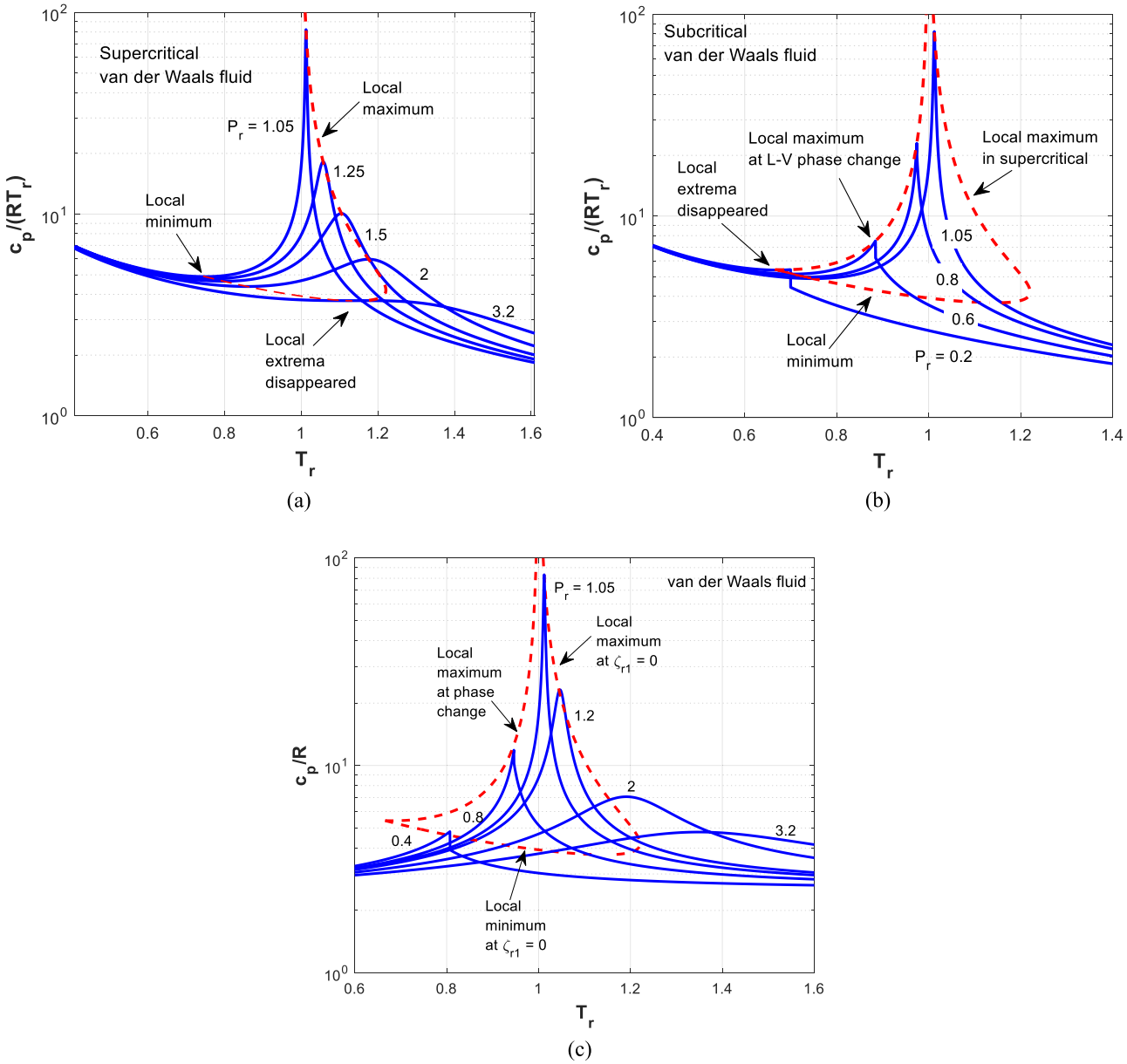

FIG. 3. Variations of (a) c_p/RT_r with temperature at $P_r > 1$, (b) c_p/RT_r at subcritical pressure, $P_r = 0.2$, 0.6, and 0.8, for reference, the supercritical curve for $P_r = 1.05$ is also included, and (c) c_p/R at $P_r = 0.4$, 0.8, 1.05, 1.2, 2, and 3.2, from subcritical to supercritical conditions for the vdW fluid.

local maximum. However, the local maximum as shown for $P_r \approx 0.6$ disappears as P_r decreases, non-existent at $P_r \approx 0.155$ [Fig. 3(b)]. Figure 3(c), in agreement with Figs. 2(a) and 2(c), shows convincingly that there exist only maxima but no minima for c_p/R, in contrast to c_p/RT_r, for the entire range of pressure from the subcritical to supercritical state. Note also that the peaks of the two specific heat functions, c_p/R and c_p/RT_r, do not occur at the same pressures and temperatures, except for the CP.

Figures 4(a) and 4(c) present the isothermal variation of c_p/RT_r and c_p/R with P_r for the supercritical and subcritical conditions, respectively. Figures 4(b) and 4(d) show the corresponding variation of $\zeta_{r2,T}$. Interestingly, one notices that $\zeta_{r2,T}$ is the isothermal derivative of c_p/RT_r with respect to pressure [Eq. (12a)] as opposed to ζ_{r1} which is the isobaric derivative with respect to temperature [Eq. (11)]. In this case, $\zeta_{r2,T}$ shows only one zero location in Fig. 4(b), as opposed to the two zero locations for ζ_{r1} in Fig. 2(b), and none in Fig. 4(d) for the subcritical condition. The discontinuity within the subcritical state, at the point of liquid-vapor phase change, is again shown in Fig. 4(c). The two sets of curves are similar and since they are discontinued at the point of phase change, there is no additional local extremum, and hence, no zero slopes are expected in the case of $\zeta_{r2,T}$ [Fig. 4(d)]. This is true only for the vdW fluid but not for the real fluids, as shown in Sec. IV F.

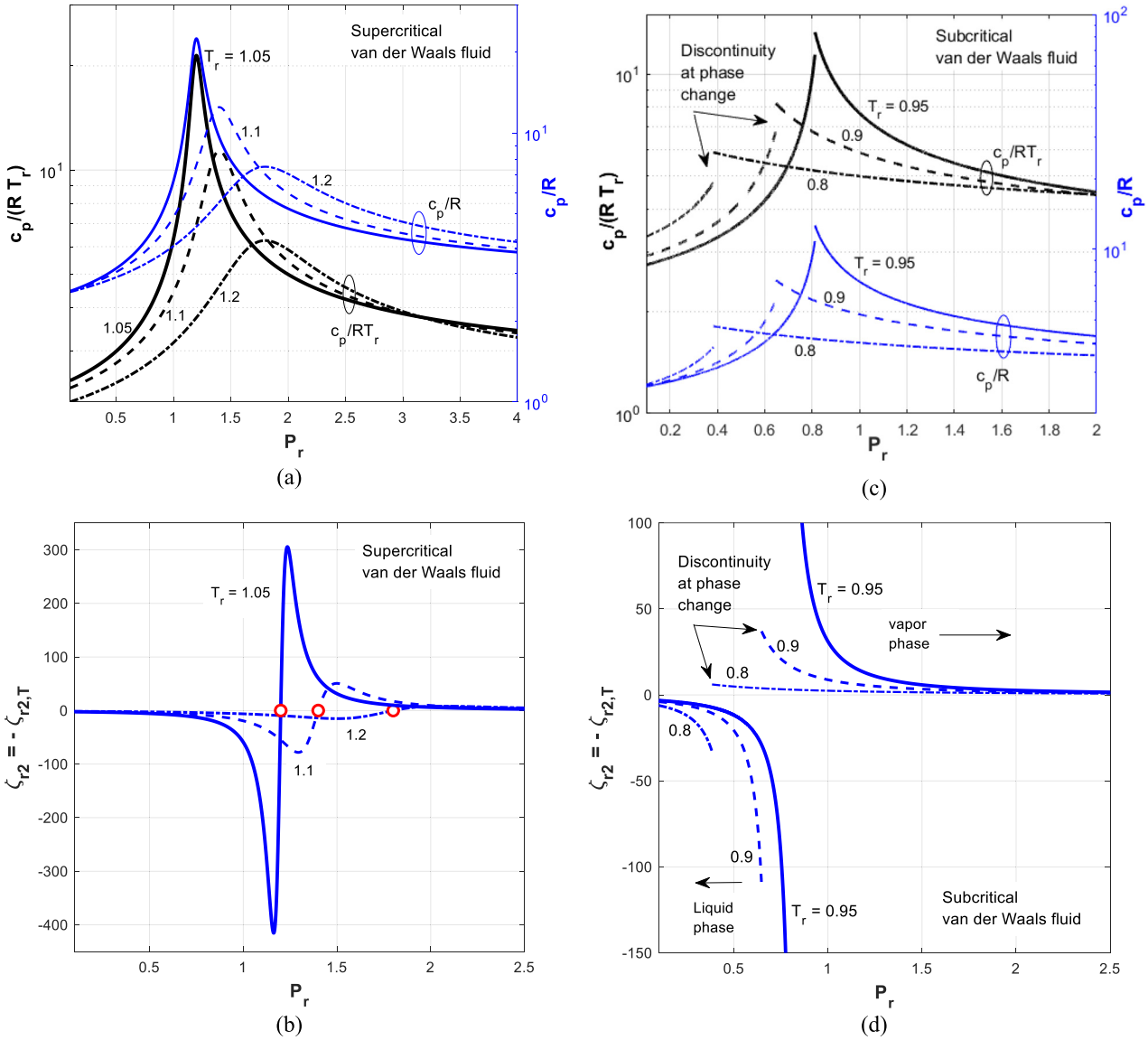

FIG. 4. Variations of (a) c_p/RT_r and c_p/R, (b) ζ_{r2} with reduced pressure P_r for $T_r = 1.05$, 1.1, and 1.2, under SC conditions ($T_r > 1$), and (c) c_p/RT_r and c_p/R and (d) ζ_{r2} ($= -\zeta_{r2,T}$) with reduced pressure P_r for $T_r = 0.8$, 0.9, and 0.95, under subcritical conditions, for the vdW fluid. Black lines are for c_p/RT_r (left axis) and blue lines for c_p/R (right axis).

In Fig. 5, the contours of c_p/RT_r show its variation with pressure and temperature; the value being the highest at CP (see the color bar). As depicted in Fig. 3(a), c_p/RT_r decreases as the pressure and/or temperature increase beyond the critical point whereas in the subcritical state, the behavior is quite complex and depends on which side of the liquid–vapor line the fluid is. Figure 5 also shows that the effect of pressure on c_p/RT_r is weak only at low reduced temperatures, say $T_r < 0.5$. Furthermore, Fig. 5 does reveal the discontinuity in c_p/RT_r at the liquid–vapor line. Another aspect of this figure is the region below the critical pressure and beyond the liquid–vapor line, the subcritical gas region. Can this state be considered a typical gas state when the property of c_p/RT_r changes significantly? Indeed, as depicted in Fig. 1 the anomalous region does extend to $T > T_{L\text{-}V}$ and $P_r < 1$.

Superposed in Fig. 5 are also the curves for the loci of $\zeta_{r2,T} = 0$ (in magenta) and $\zeta_{r1} = 0$, red representing $(c_p/RT_r)_{p,\min}$ and blue $(c_p/RT_r)_{p,\max}$. [Throughout this paper, subscript p to the governing parameters indicates that the extrema are obtained following an isobaric process while subscript T indicates that they are obtained following an isothermal process.] The curve for $\zeta_{r1} = 0$ forms a closed loop with the liquid–vapor line as part of its boundary, while the curve for $\zeta_{r2,T} = 0$ extends without any bound, starting from the CP, to be discussed in Sec. IV F. The curve for $\zeta_{r1} = 0$ starts in the subcritical state at $P_r \approx 0.155$ and $T_r \approx 0.664$ and has an inflexion point (peak) at $P_r \approx 3.227$ and $T_r \approx 1.140$, with the slope being zero there; the maximum temperature to which this loop extends is $T_r \approx 1.22$.

The contour map of c_p/RT_r in Fig. 5 identifies the possible region where the anomalous behavior of thermodynamic properties may occur. The loop of zero ζ_{r1} encloses a region where an inversed variation of the isobaric slope of c_p/RT_r exists, as also indicated in Figs. 3(a)–3(c). Within this loop, the contour lines increase with T_r, instead of decreasing outside of the loop. The region is bounded on the left by $(c_p/RT_r)_{p,\min}$ and on the right by $(c_p/RT_r)_{p,\max}$. Such abnormal shape of curves disappears at high pressure, $P_r > 3.2$. The anomalous behavior of c_p/RT_r continues further outside of the right boundary and finally reaches the maximum points of the isothermal slope of c_p/RT_r, see the line $(c_p/RT_r)_{T,\max}$ along isobaric lines in the supercritical region ($P_r > 1$). In the subcritical region, however, the loop is bounded by the L–V line. The dense contours appearing in the vicinity of the critical point, however, indicate that the anomalous behavior extends well into the gas phase ($P_r < 1$) and the supercritical gas-like state when $P_r > 1$.

The behavior of c_p/RT_r in Fig. 5 can be better visualized in Fig. 6 where its three-dimensionality with respect to P_r and T_r are presented; each color band represents values in a range of c_p/RT_r. Note that Imre *et al.*[1] and Wagner and Kruse[41] had presented black and white 3D plots of c_p for water but, to the authors knowledge, no other 3D plots are reported in the literature. From Figs. 5 and 6, it is evident that the highest value of c_p/RT_r exists at $P_r = 1$ and $T_r = 1$. The spread is clearly from the deep into the subcritical region to much beyond the CP, in the SC region. This demonstrates convincingly that the liquid-like (SCLL) behavior in the supercritical region, which many authors have demonstrated in the last 25 years, does not start uniquely at the critical point, but far below it. Indeed, it begins between the triple point and the critical point; at $P_r \approx 0.155$ and $T_r \approx 0.664$ in the case of vdW fluid. This is the point P, shown hypothetically in Fig. 1.

These 3D plots (Fig. 6) display extremely well the complex behavior of the fluid in the region around CP, in both the supercritical and subcritical regions. The parallel lines with almost equal gap in between [Figs. 6(b)–6(d)] exhibit splendidly the monotonous behavior of

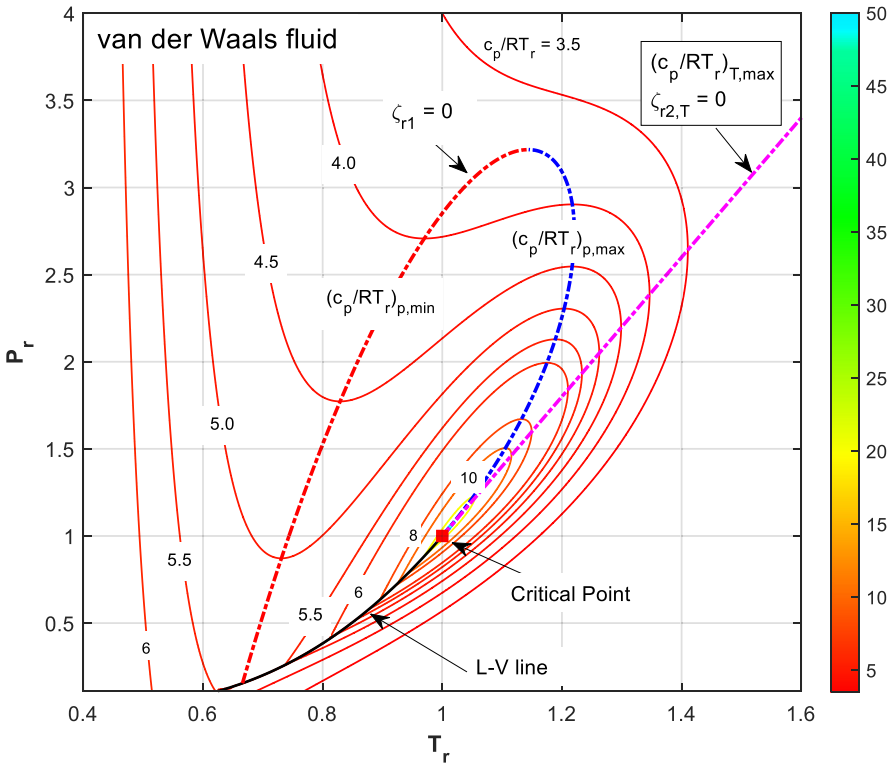

FIG. 5. Contours of isobaric specific heat parameter c_p/RT_r in $P_r - T_r$ plane for its values from 3.5 to 50 (the curves after ten are not labeled); the maximum value centered at the CP. There is a discontinuity at the liquid–vapor line. Superposed are two curves that connect the loci of $\zeta_{r1} = 0$ and $\zeta_{r2,T} = 0$, representing the extrema of the curves of c_p/RT_r [red dashed line for minimum, blue for maximum, and magenta line for $(c_p/RT_r)_{T,\max}$, or $\zeta_{r2,T} = 0$]. Note that the data for liquid–vapor line for vdW fluid are taken from Johnston.[34] In all of the figures, the subscript p to the governing parameters indicates that the extrema are obtained following an isobaric process while subscript T indicates that they are obtained from an isothermal process.

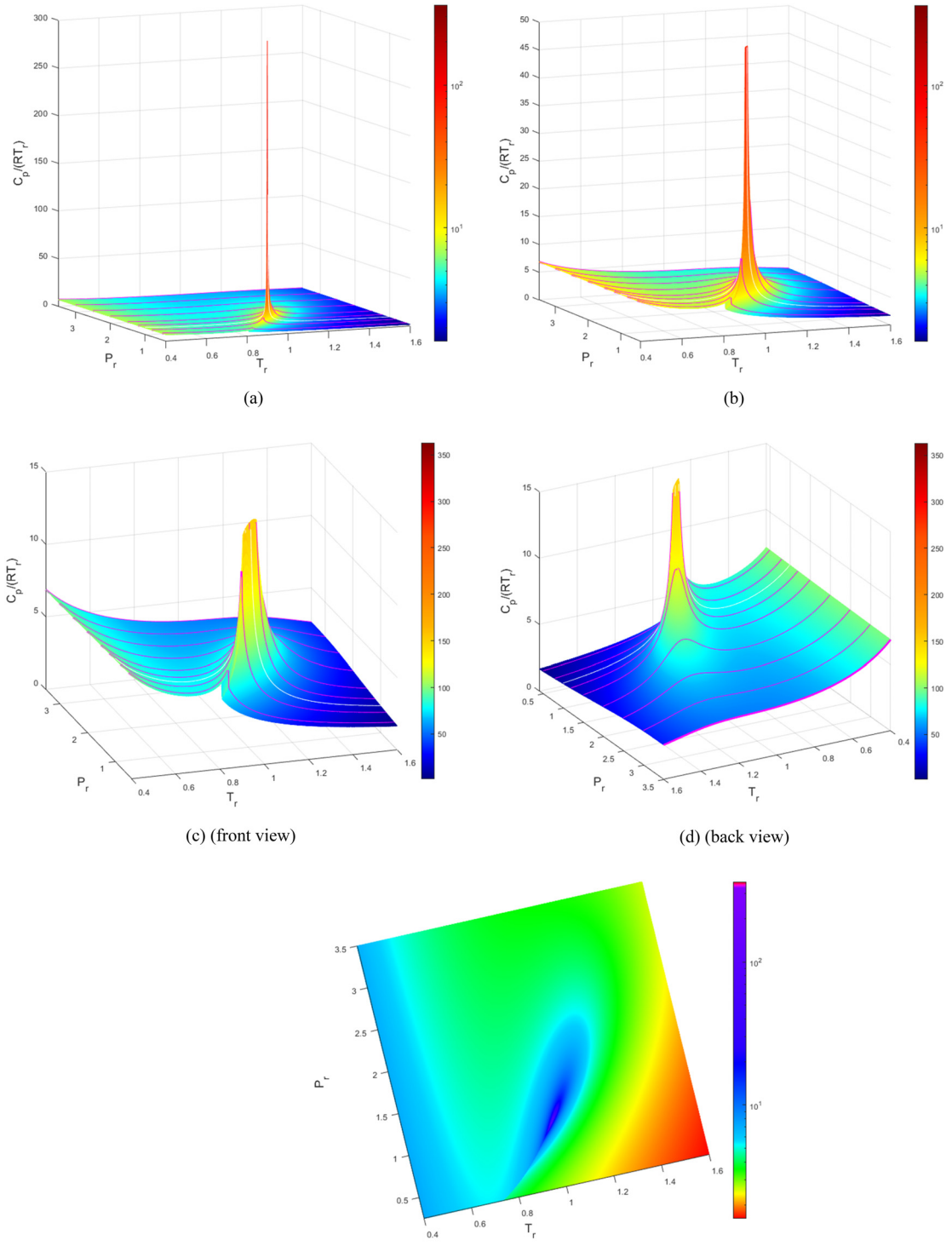

FIG. 6. Three-dimensional images of isobaric specific heat parameter $c_p/(RT_r)$ for the vdW fluid, with respect to P_r and T_r, (a) view from the corner of P_r and T_r axes, (b) truncated view from the corner of P_r and T_r axes, (c) front view from the $P_r = 0$ plane, (d) back view from the $P_r = 3.5$ plane, and (e) view from the top. The top has been truncated in (b)–(d) to show the spread.

c_p/RT_r far away from the CP on both sides. The most revealing aspect of these 3D images is presented in Fig. 6(e), where the blue color encompassing $(c_p/RT_r)_{max}$ shows a close to the elliptical shape, as hypothesized in Fig. 1.

B. Isobaric volumetric expansion parameter ($v_r\beta T_c$)

When $v_r\beta T_c$ is plotted against the reduced pressure, P_r, we again find the existence of two extrema, minima on the left, $P_r < 1$, and maxima on the right, $P_r > 1$ [Fig. 7(a)], which disappear at the high reduced temperatures, T_r. Interestingly, the (βT_c) again misses to show this behavior and exhibit only one maximum at $P_r > 1$. As can be expected, ζ_{r3} reveals two zero points [Fig. 7(b)]. Furthermore, the curves for βT_c in subcritical state [Fig. 7(c)] exhibit only a local maximum at the point of phase change whereas $v_r\beta T_c$ shows both a local maximum at the phase change and a local minimum left to it; this local minimum disappears at low T_r. Corresponding to the cases in Fig. 7(c), ζ_{r3} shows only one zero location, for the local minimum of $v_r\beta T_c$ [Fig. 7(d)], and exhibits discontinuity at the phase change. Although not shown here, the plots for both (βT_c) and $(v_r\beta T_c)$ against reduced temperature, T_r (isobaric lines), and consequently, ζ_{r2}-curve show only one zero location when plotted against T_r.

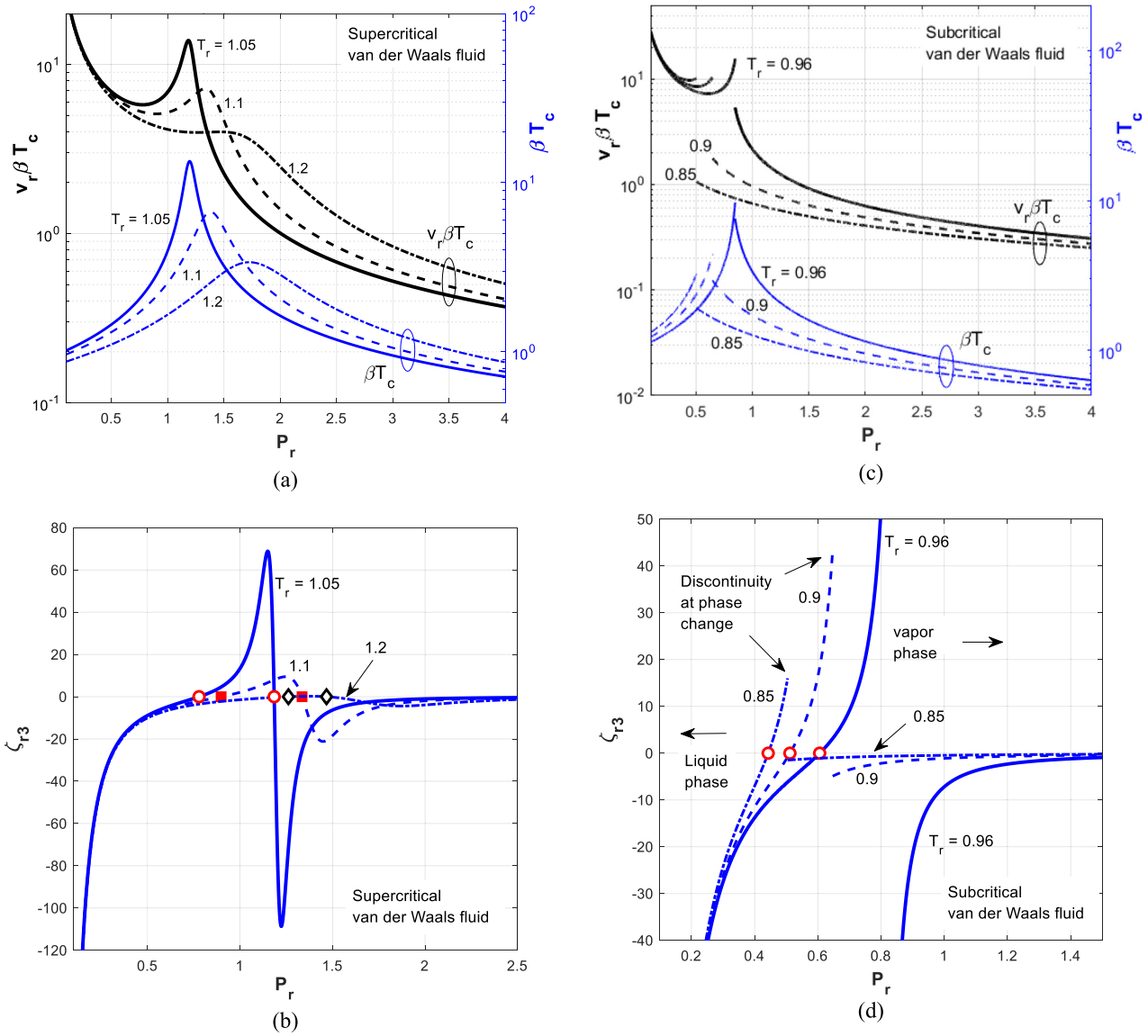

FIG. 7. Variations in (a) $v_r\beta T_c$ (black line on left axis) and βT_c (blue line on right axis), and (b) ζ_{r3} vs P_r at $T_r = 1.05$ (blank circle), 1.1 (red square), and 1.2 (blank diamond), under SC conditions, (c) $v_r\beta T_c$ and βT_c, and (d) ζ_{r3} vs P_r at $T_r = 0.85$, 0.9, and 0.96, under subcritical conditions, for the vdW fluid.

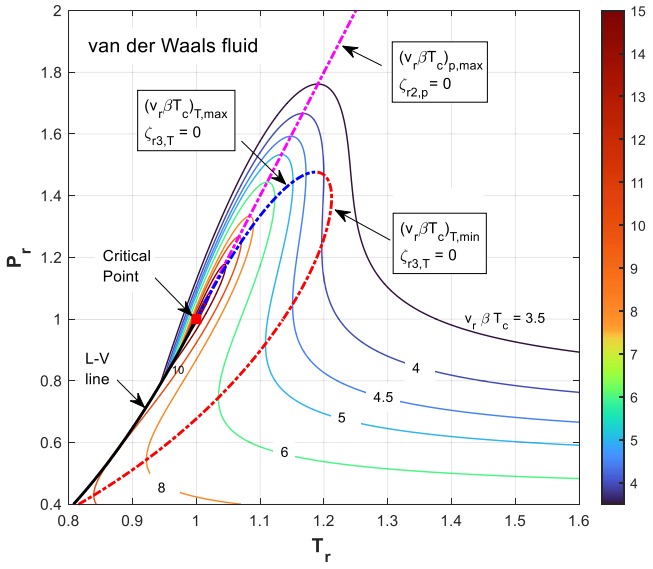

(a)

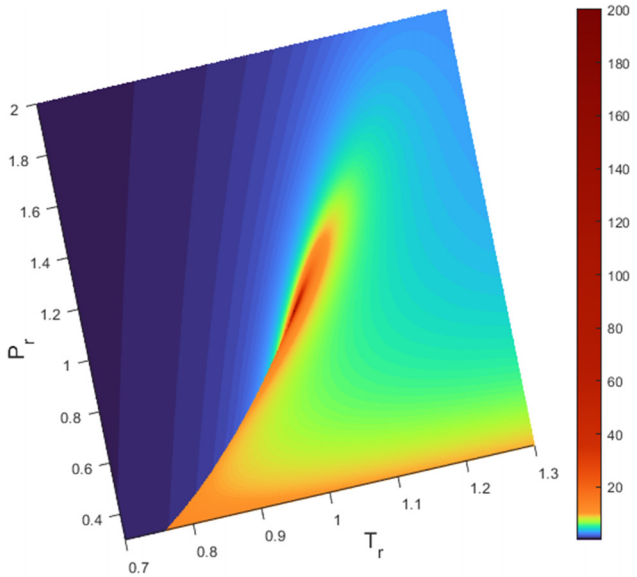

(b)

FIG. 8. (a) Contours of function $v_r\beta T_c$ in $P_r - T_r$ plane for its value above 3.5 (curves after ten are not labeled.); the maximum value centers at the CP. Superposed are the two curves that connect the loci of $\zeta_{r2,p} = 0$ and $\zeta_{r3,T} = 0$, representing the extrema of the curves of $v_r\beta T_c$ along both isobaric line and isothermal lines, red dashed line for $(v_r\beta T_c)_{T,min}$, blue dashed line for $(v_r\beta T_c)_{T,max}$, and magenta for $(v_r\beta T_c)_{p,max}$ and $\zeta_{r2,p} = 0$, and (b) three-dimensional image of $v_r\beta T_c$, viewed from the top.

The contours of $v_r\beta T_c$ are presented in Fig. 8(a) together with the loci of $\zeta_{r2,p} = 0$ and $\zeta_{r3,T} = 0$, representing the extrema of the curves of $v_r\beta T_c$ along both isobaric and isothermal lines. The line for $\zeta_{r2,p} = 0$ ($v_r = 1$ and $P_r = 4T_r - 3$), extending beyond any bound on the upper side, is the same as that for $\zeta_{r2,T} = 0$ in Fig. 5 for $(c_p/T_rR)_{T,max}$. On the other hand, the curve for $\zeta_{r3,T} = 0$ forms a loop on the right side of the L-V/$\zeta_{r2} = 0$ line. Similar to that observed in Fig. 5, the lines for constant $v_r\beta T_c$ show discontinuity at the L-V line. However, the peaks along an isobaric line in the present case are given by

$$(v_r\beta T_c)_{p,max} = \left(\frac{\partial v_r}{\partial T_r}\right)_{P_r,max} = \frac{2}{3(T_r - 1)} = \frac{8}{3(P_r - 1)}, \quad (36)$$

which lies on the isochoric line, $v_r = 1$ and $\zeta_{r2} = 0$. The inflexion point of the loop for $\zeta_{r3,T} = 0$ is at $P_r \approx 1.494$, and the maximum temperature to which the loop extends to is $T_r \approx 1.21$, a value almost identical to what was observed for c_p/T_rR.

This $(v_r\beta T_c)_{p,max}$ line defines a phase transition from a liquid-like to a gas-like phase in the SC state ($P > P_c$), with both the specific volume and entropy changing continuously and smoothly. This phase transition is represented by the loci of the zeros of third-order cross-derivative of the Gibbs free energy, $(\partial^3 g/\partial T^2 \partial P) = 0$, or $\zeta_{r2} = 0$, which together with the liquid–vapor curve, gives a unified view of the liquid-to-gas transition. Below the critical point, the liquid-to-gas phase change is the phase-transition with distinct changes in all thermodynamic properties including the specific volume and entropy. However, above the critical point, it is a phase transition from the liquid-like to gas-like states. Indeed, the $(v_r\beta T_c)_{p,max}$ line divides the entire fluid region (above the triple point) into two regions, liquid (or liquid-like) and gas (or gas like).

Similar to Fig. 5, Fig. 8(a) reveals the region of highly deformed contours of $v_r\beta T_c$ near the critical point, but major changes occur in the gas phase ($P_r < 1$) or SCGL ($P_r > 1$), i.e., on the right-hand side of the L–V line and the line of $\zeta_{r2,p} = 0$, contrary to the loop for c_p/RT_r. The top view of $(v_r\beta T_c)$ in the 3D plot [Fig. 8(b)] exhibits the spread of this parameter; the changes are large in the red-yellow region and weaker outside of it. However, from Figs. 8(a) and 8(b), it is evident that the change in this parameter is appreciable until $T_r \approx 1.15$.

C. Isothermal compressibility parameter ($v_r\kappa P_c$)

Figure 9(a) presents the variations in $v_r\kappa P_c$ and κP_c against the reduced temperature, for $P_r = 1.05$, 1.2, and 1.4. Here again, we observe that κP_c has only one local extremum, the maxima, whereas $v_r\kappa P_c$, have both local minimum and local maximum; however, both extrema eventually disappear at high pressures. Consequently, ζ_{r3} in Figs. 9(b) and 9(c) exhibit two zero locations.

The variations in $v_r\kappa P_c$ and κP_c against P_r are presented in Fig. 10(a) for $T_r = 1.01$, 1.05, 1.15. We observe two extrema (on the isothermal line) in the case of $v_r\kappa P_c$, one minimum in the subcritical state and the other maximum in the SC state. Both local extrema eventually disappear at high temperatures. Corresponding to the case of $T_r = 1.05$ in Fig. 10(a), the curve for ζ_{r4} in Fig. 10(b) shows two zero locations. Note that $v_r\kappa P_c$ exhibit two extrema and two zero points on both isothermal and isobaric plots like the c_p/RT_r, but unlike $v_r\beta T_c$.

The contours of $v_r\kappa P_c$ are presented in Fig. 11 together with the loci of $\zeta_{r3} = 0$ and $\zeta_{r4} = 0$, representing the extrema of $v_r\kappa P_c$ along both isobaric and isothermal lines; the loop for $\zeta_{r3} = 0$ is similar to that in Fig. 8. Again, $\zeta_{r4} = 0$ forms a loop only on the right side of L–V/

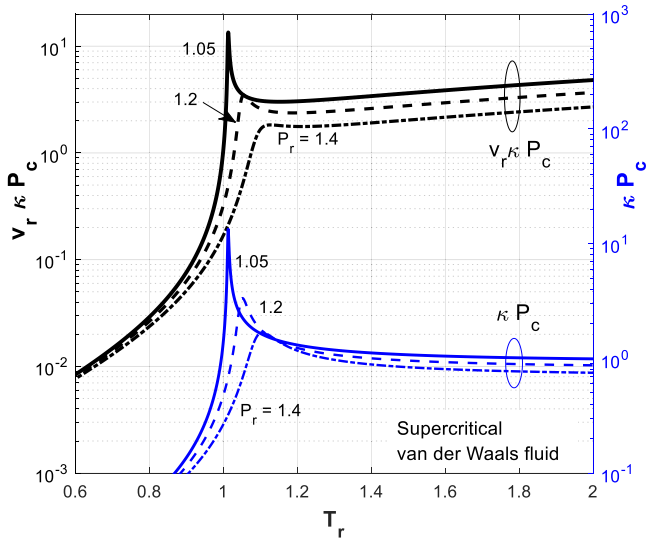

(a)

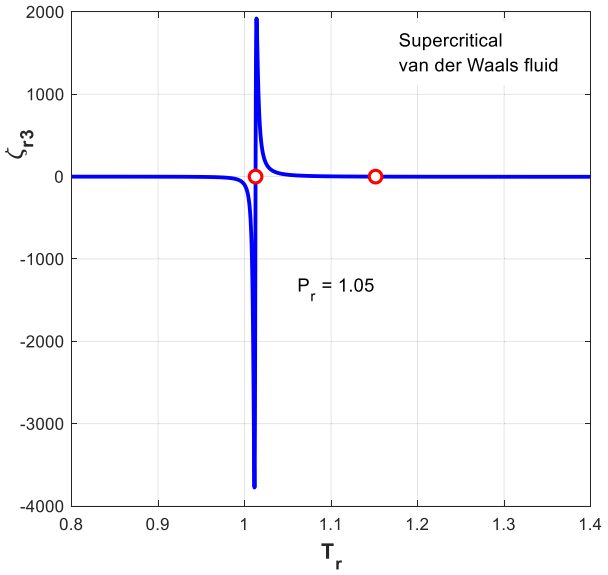

(b)

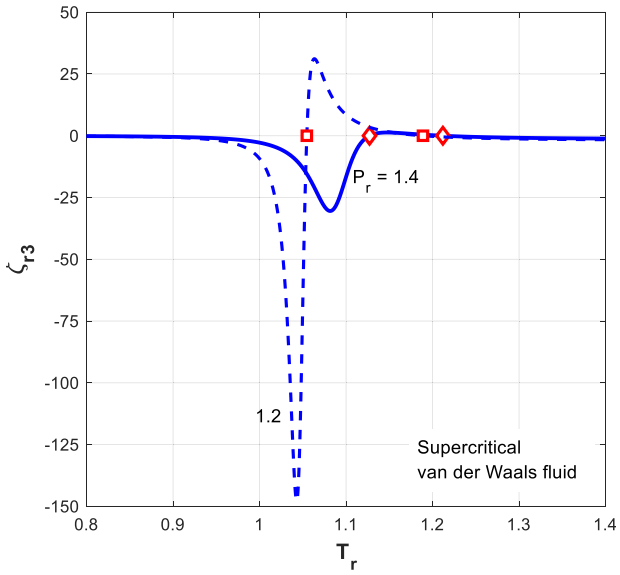

(c)

FIG. 9. Variations of (a) $v_r\kappa P_c$ (black line on left axis) and κP_c (blue line on right axis) with reduced temperature T_r at $P_r = 1.05$, 1.2, and 1.4, under SC conditions, (b) ζ_{r3} vs reduced temperature $T_r = 1.05$, and (c) $T_r = 1.2$ and 1.4, under SC conditions for the vdW fluid.

$\zeta_{r2} = 0$ line. Similar to what we observed in Figs. 5 and 8, the lines for constant $v_r\kappa P_c$ show discontinuity at the L–V line. The peak pressure for $\zeta_{r4} = 0$ loop is $P_r \approx 1.18$, and the maximum temperature to which this loop extends to is $T_r \approx 1.07$. The general trend of the variation in $v_r\kappa P_c$ in Fig. 11 is that it decreases as the pressure increases, in both the subcritical and supercritical regions. It shows the peak at $\zeta_{r4} = 0$ (red) and then inflexion to lower values, before it again starts increasing at high T_r. Interestingly, the loop of $\zeta_{r4} = 0$ is completely subsumed by the loop of $\zeta_{r3} = 0$.

D. The complete phase diagram for vdW fluid and the anomalous region

Finally, we can track the extrema of (c_p/RT_r), $(v_r\beta T_c)$, and $(v_r\kappa P_c)$ for the van der Waals fluid by plotting the loci of $\zeta_{ri} = 0$, $i = 1$, 2, 3, and 4 (Fig. 12) and summarize the overall behavior. For simplicity and better understanding, we have used the dimensional parameters, i.e., c_p/T, $v\beta$, and $v\kappa$, in Fig. 12. As noted earlier, the $(v\beta)_{p,\max}$ line, which is also the line of $(c_p/T)_{T,\max}$, follows exactly the critical isochoric line, $v_r = 1$ for

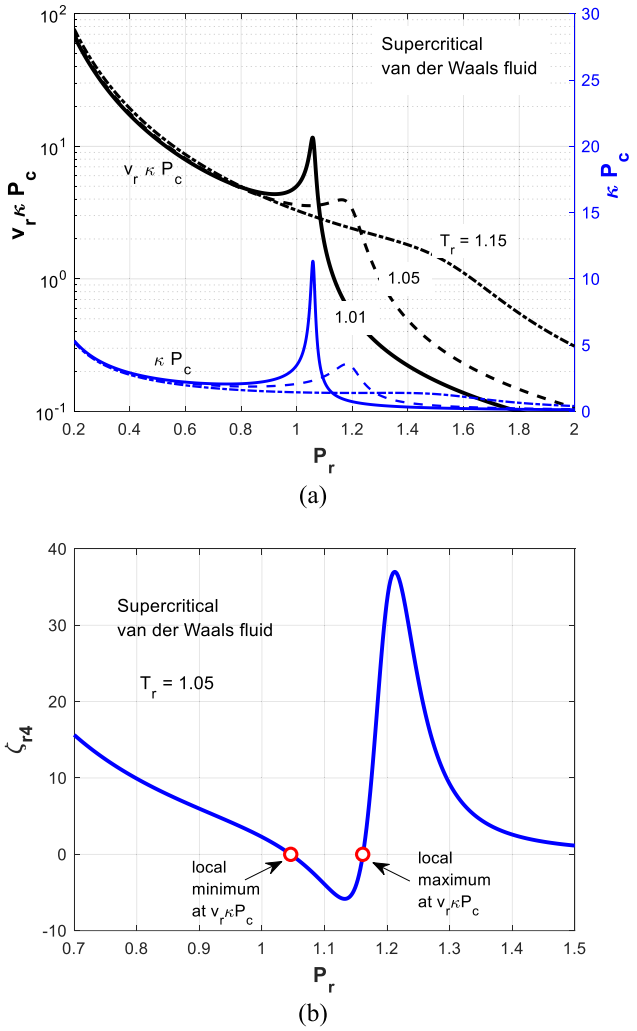

FIG. 10. Variations of (a) $v_r \kappa P_c$ (black line, left axis) and κP_c (blue line, right axis) with P_r at $T_r = 1.01$, 1.05, and 1.15, under SC conditions, and (b) ζ_{r4} vs reduced pressure P_r at $T_r = 1.05$, for the vdW fluid.

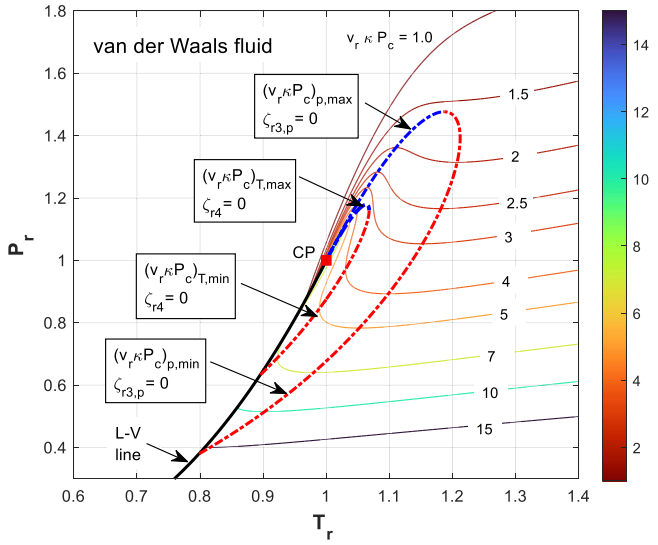

FIG. 11. Contours of the function $v_r \kappa P_c$ in the (P_r, T_r) plane from 1 to 15 for the vdW fluid. The maximum values are collapsed to the L-V line in the subcritical state. Two loops are formed, one is the loci of $\zeta_{r3,p} = 0$ and one for $\zeta_{r4} = 0$. For the loop of $\zeta_{r3,p} = 0$, red dashed line for $(v_r \kappa P_c)_{p,min}$ and blue dashed line for $(v_r \kappa P_c)_{P,max}$. The loop of $\zeta_{r4} = 0$ is totally within the loop of $\zeta_{r3,p} = 0$.

$\zeta_{r2} = 0$. It passes through the critical point, and separates the liquid-like and gas-like states. On the left side of this line is $(c_p/T)_{p,min}$ in red and $(c_p/T)_{p,max}$ in blue for $\zeta_{r1} = 0$. Note that most part of $(c_p/T)_{p,min}$ is in the region of $T_r < 1$ even though the pressure goes much beyond the critical pressure, $P_r \geq 1$. As noted earlier, the SCLL behavior starts quite early in the subcritical regime, at $P_r \approx 0.155$ and $T_r \approx 0.664$. When we consider the loops of $(v\beta)$ and $(v\kappa)$, i.e., $\zeta_{r3} = 0$ and $\zeta_{r4} = 0$, we find that the effect of $(v\kappa)$ starts much later, it is highly localized, and the loop of $\zeta_{r4} = 0$ is completely subsumed by the loop of $\zeta_{r3} = 0$. The loop of $\zeta_{r3} = 0$ starts at $P_r \approx 0.4$ and $T_r \approx 0.8$ and ends at $P_r \approx 1.5$ and $T_r \approx 1.23$.

In Fig. 12, the Widom lines for the dimensional properties, c_p, β, and κ, are superposed over the plots for $\zeta_{ri} = 0$. Interestingly, these lines for $c_{p,max}$, β_{max}, and κ_{max}, all lie between the loops for $\zeta_{r1} = 0$ and $\zeta_{r3} = 0$ and the line for $\zeta_{r2} = 0$ passes through this zone. The region between the loops for $(c_p/T)_{p,min,max}$ and $(v\beta)_{T,min,max}$ is where the Widom delta starts, originating from the critical point. As noted by Imre *et al.*,[22] the Widom lines for all thermophysical properties may lie within the Widom delta. Here, it may be worthwhile to note that an analogous, maximum and sigmodal-like change with inflection was reported in the context of Widom anomalies for argon.[22] In addition, Ha *et al.*[26] and Yoon *et al.*[27] have observed recently that both the liquid-like and gas-like fluids may co-exist within this delta.

Lastly, we can map the anomalous region quantitatively using the boundaries of the closed loops and knowledge on the Widom delta (Fig. 12). It is bounded (a) at the bottom, by the intersection of $(c_p/T)_{p,min}$ and the liquid–vapor line (point A), (b) on the left, by the line for $(c_p/T)_{p,min}$, red line AB, (c) on the top, by the highest pressure line that is tangent to $\zeta_{r1} = 0$ curve and intersects the isochoric, $\zeta_{r2} = 0$ line (dashed green line BC), (d) on the right side bottom, the curve for $(v\beta)_{T,min}$ or $(v\kappa)_{p,min}$ (red line AD), and (e) on the upper side of the right, by the tangent to $\zeta_{r3} = 0$ curve that intersects the isochoric, $\zeta_{r2} = 0$ line at C (dashed green line DC). Thermodynamically, the anomalous region ABCDA includes the Widom delta. The top boundary of highest pressure, $P_{r,max} = 3.227$, can be justified since it is the upper limit of the anomalous region beyond which the importance of the Widom line goes down; Banuti[28] had suggested $P_r \approx 3$. Although a thermodynamic justification of line DC is not readily available, an inspection of the isobaric lines of specific heat on c_p-vs-T plots of Ar, CH_4, N_2, CO_2, and water, indicates that no large-scale variations occur beyond $T_{r,max}$ (point C) for $P_r < P_{r,max}$ (see Sec. IV E).

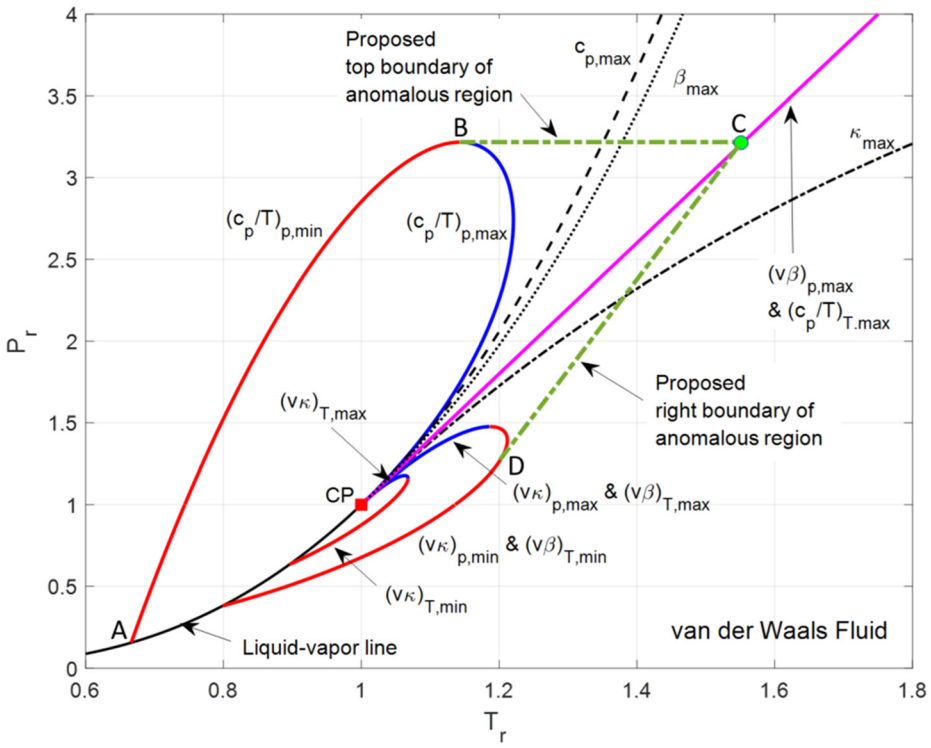

FIG. 12. Loops formed in the (P_r, T_r)-plane from the three third-order functions: $\zeta_{r1} = 0$, $\zeta_{r3} = 0$, and $\zeta_{r4} = 0$. The loci of $\zeta_{r2} = 0$, however, extend beyond the critical point without any bound. Three Widom lines, $c_{p,max}$, β_{max}, and κ_{max}, are also superposed on the $P_r - T_r$ map. Two dashed green lines are proposed at the top and on the right; the top being the line for $P_{r,max} = 3.227$, from $T_r = 1.140$ to 1.494, intersecting the line of $\zeta_{r2} = 0$ and the right boundary is tangent to the line of $\zeta_{r3} = 0$ at approximately $T_r = 1.172$ and $P_r = 1.138$. The green lines together with the curves for $(c_p/T)_{p,min}$ and $(v\beta)_{T,min}$ form the anomalous region. (Note that to make the plot less crowded, we have labeled the curves with dimensional form of modified parameters, instead of the reduced, dimensionless form.)

E. Anomalous regions for argon, methane, nitrogen, carbon dioxide, and water

In this section, we present the results for argon, methane, nitrogen, carbon dioxide, and water. Argon is considered first since it is a noble fluid and behaves similar to the van der Waals fluid. Figure 13(a) shows the contours of c_p/RT_r; the value again being the highest at the critical point. The pattern of the contours with maxima and minima in Fig. 13(a) is identical to that observed for the vdW fluid in Fig. 5. Superposed in Fig. 13(a) are also the curves for the loci of $\zeta_{r2,T} = 0$ (in magenta) and $\zeta_{r1} = 0$, red representing $(c_p/RT_r)_{p,min}$ and blue $(c_p/RT_r)_{p,max}$. The curve for $\zeta_{r1} = 0$ again forms a closed loop with the liquid–vapor line as part of its boundary. It starts in the subcritical state at $P_r \approx 0.173$ and $T_r \approx 0.730$ [point A in Fig. 13(b)] and has an inflexion point (peak) at $P_r \approx 3.640$ and $T_r \approx 1.094$ (point B) with the slope being zero there. The maximum temperature to which this curve extends to $T_r \approx 1.22$.

The above trends of the vdW fluid (Figs. 5 and 12) and argon [Figs. 13(a) and 13(b)] are replicated by CH_4, N_2, and CO_2 [Figs. 14(a), 15(a), and 16(a)] as well as by the water [Figs. 17(a) and 17(b)]. The starting point of the curve for $\zeta_{r1} = 0$, for all fluids considered here, is given in Table I as point A, (P_r, T_r) being (0.173, 0.730) for Ar, (0.199, 0.768) for CH_4, (0.192, 0.772) for N_2, (0.203, 0.801) for CO_2, and (0.144, 0.788) for water. Clearly, the values for all fluids are close to each other; the outlier being the water with P_r somewhat lower. This trend is also followed by the peak values (point B); (3.446, 1.101) for CH_4, (3.383, 1.088) for N_2, (3.252, 1.086) for CO_2; again, the water (4.630, 1.108) has higher P_r. Interestingly, all $(c_p/RT_r)_p$ loop extends to the maximum temperature of $T_r \approx 1.15$, except for CO_2, for which it is ~1.12.

The contours of $v_r\beta T_c$ and $v_r\kappa P_c$ for all real fluids (not presented here) show similar behavior as demonstrated for the vdW fluid in Figs. 8(a) and 11, respectively. Indeed, the loops formed by the curves for expansion parameter, $(v_r\beta T_c)_{T,max}$ and $(v_r\beta T_c)_{T,min}$ ($\zeta_{r3,T} = 0$) and compressibility parameter, $(v_r\kappa P_c)_{T,max}$ and $(v_r\kappa P_c)_{T,min}$ again lie on the right side of the L-V/$\zeta_{r2} = 0$ line, as shown in Figs. 13(b), 14(a), 15(a), 16(a), and 17(b) for Ar, CH_4, N_2, CO_2, and water, respectively. Indeed, these figures present all three loops together, the truncated part of the line for $\zeta_{r2} = 0$ (to be discussed in Sec. IV F), and the Widom lines for the dimensionless properties, c_p/R, βT_c, and κP_c lie between the loops for $\zeta_{r1} = 0$ and $\zeta_{r3} = 0$.

Furthermore, the characteristics of these curves are identical to those observed in Fig. 12 for the vdW fluid. As noted earlier, ABCDA represents the area of the anomalous region. Following the previous observations on A and B and noting that the values of P_r at B and C are identical, it can be observed that the values of P_r at D and T_r at C and D do not vary much among these fluids, including water. Since the variations are not large, we can conclude that the law of corresponding states is applicable to the anomalous regions of all real fluids considered here. The exception is water, which is a polar fluid with much higher P_c, T_c, and ω (acentric factor). de Jesús *et al.*[42] have also observed a similar behavior that Widom lines for argon, nitrogen, and oxygen follow a two-parameter corresponding states whereas water and carbon dioxide deviate from them, water more than CO_2.

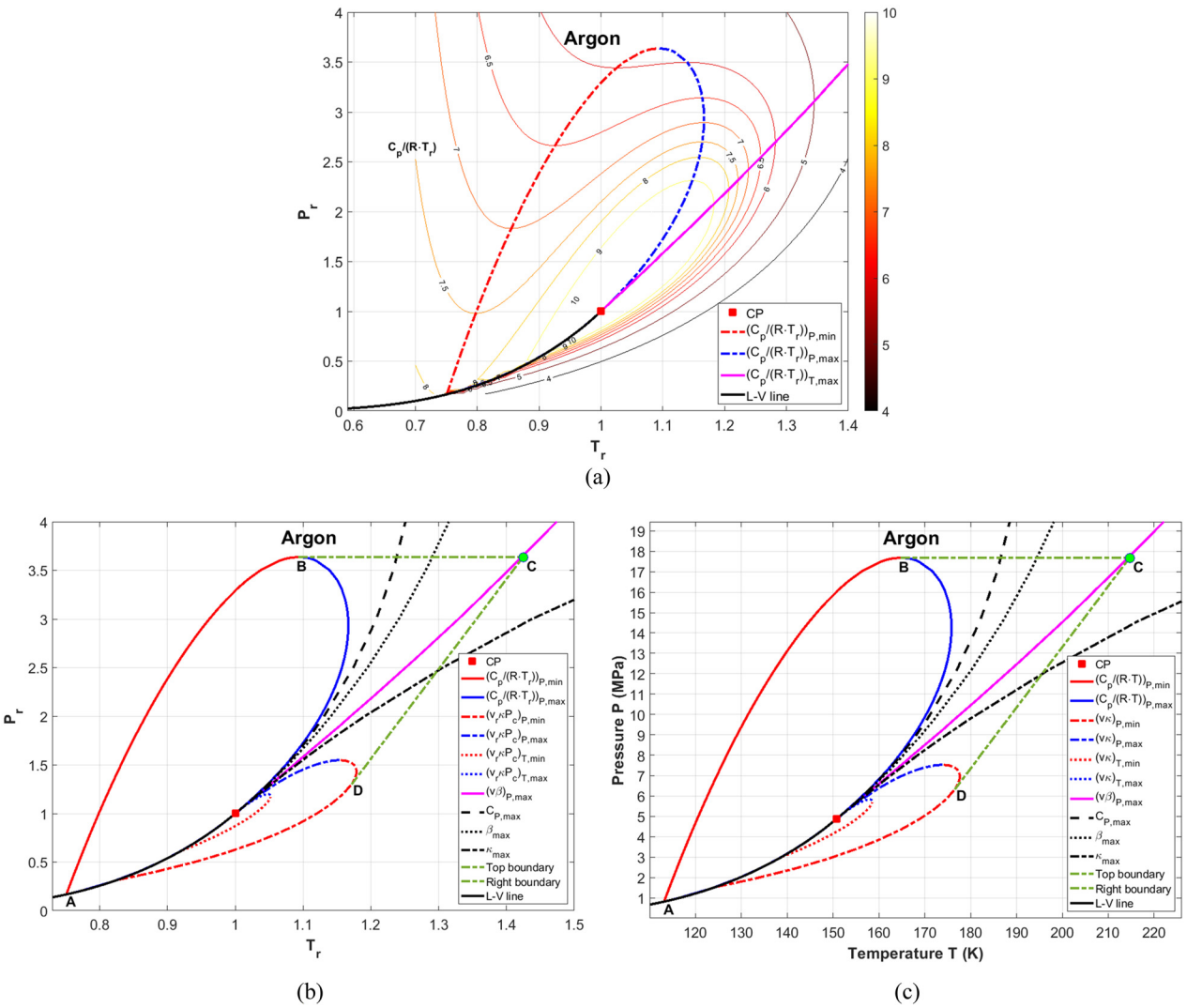

FIG. 13. Closed loops formed by the derivatives of Gibbs free energy for argon: (a) contours of c_p/RT_r, superposed are two curves that connect the loci of $\zeta_{r1} = 0$ and $\zeta_{r2,T} = 0$, representing the extrema of the curves of c_p/RT_r red dashed line for minimum, blue for maximum, and magenta for $(c_p/RT_r)_{T,max}$, and $\zeta_{r2,T} = 0$; compare with Fig. 5 for the vdW fluid and (b) three closed loops formed by $\zeta_{r1} = 0$, $\zeta_{r3} = 0$, and $\zeta_{r4} = 0$ (see Fig. 19 for the loci of $\zeta_{r2} = 0$). Three Widom lines for $c_{p,max}$, β_{max}, and κ_{max} are superposed on this $P_r - T_r$ map. Two dashed green lines are proposed at the top and on the right; the top being the horizontal line. The values of A, B, C, and D are given in Table I. (c) replica of (b) in pressure, P (MPa) and temperature, T (K); the numerical values of A–D are given in Table II.

In order to show the real values of A, B, C, and D, in pressure, P (MPa), and temperature, T (K), replicas of Fig. 13(b), 14(a), 15(a), 16(a), and 17(b) are presented in Fig. 13(c), 14(b), 15(b), 16(b), and 17(c) with the corresponding numerical values listed in Table II, together with their P_c and T_c. Again in real terms, the pressure and temperature of Point A (the start of anomalous region on the L–V line) are much below the critical pressure and critical temperature.

We also present a summary plot (Fig. 18) that demonstrates how the phase-diagram for water can be modified to include the anomalous state and the various phase transitions within this region. Note that isobaric $(\nu\beta)_{max}$ is the same as isothermal $(c_p/T)_{max}$ and isothermal $(\nu\beta)_{max}$ is equal to the isobaric $(\nu\kappa)_{max}$ (Eq. (15)). Figure 18 exhibits the various states of water in both the subcritical and supercritical regimes. Similar modifications can be made to the phase diagrams of Ar, CH_4, N_2, and CO_2 using the data in Figs. 13(c), 14(b), 15(b), and 16(b) and Table II.

The above figures clearly exhibit extension of the anomalous states deep into the supercritical fluid region, an area of considerable investigation by the SC fluid researchers. What has not been fully characterized and well understood is the liquid and vapor/gas regions on the subcritical side. We believe, the information in these figures and Table II would be very useful to scientific research and engineering applications of the SC fluids, and also, of the subcritical liquid and vapor in the regions close to the L-V line.

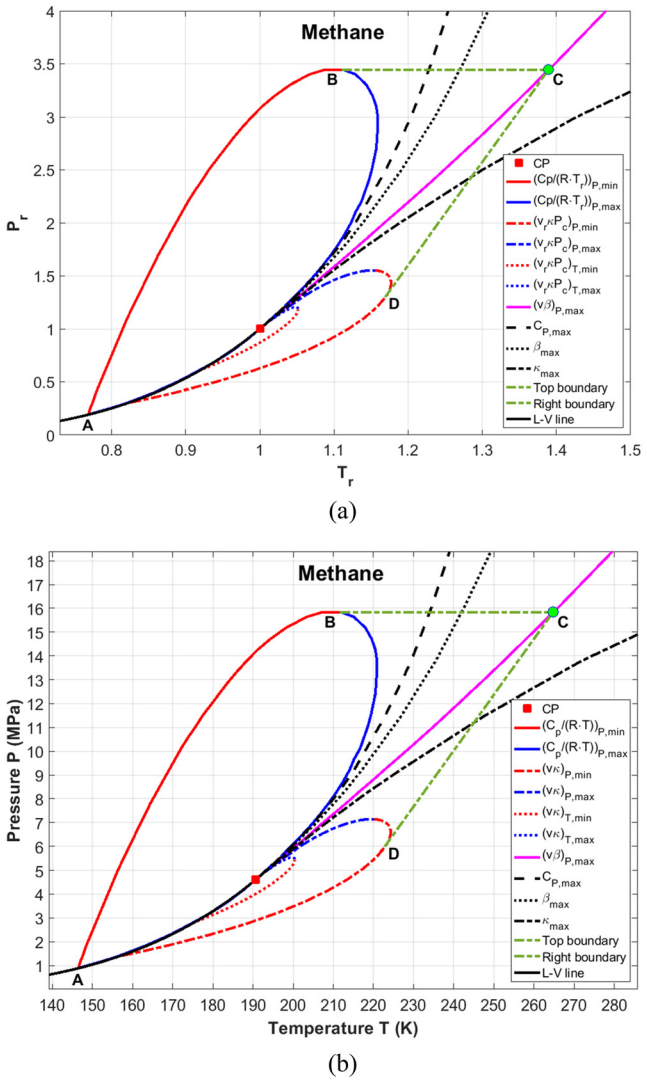

FIG. 14. Closed loops formed by the derivatives of Gibbs free energy for methane: (a) closed loops formed by the three third-order functions: $\zeta_{r1} = 0$, $\zeta_{r3} = 0$, and $\zeta_{r4} = 0$. Three Widom lines for $c_{p,max}$, β_{max}, and κ_{max} are superposed on this $P_r - T_r$ map and (b) replica of (a) in pressure, P (MPa) and temperature, T (K); the values of A–D are given in Table II.

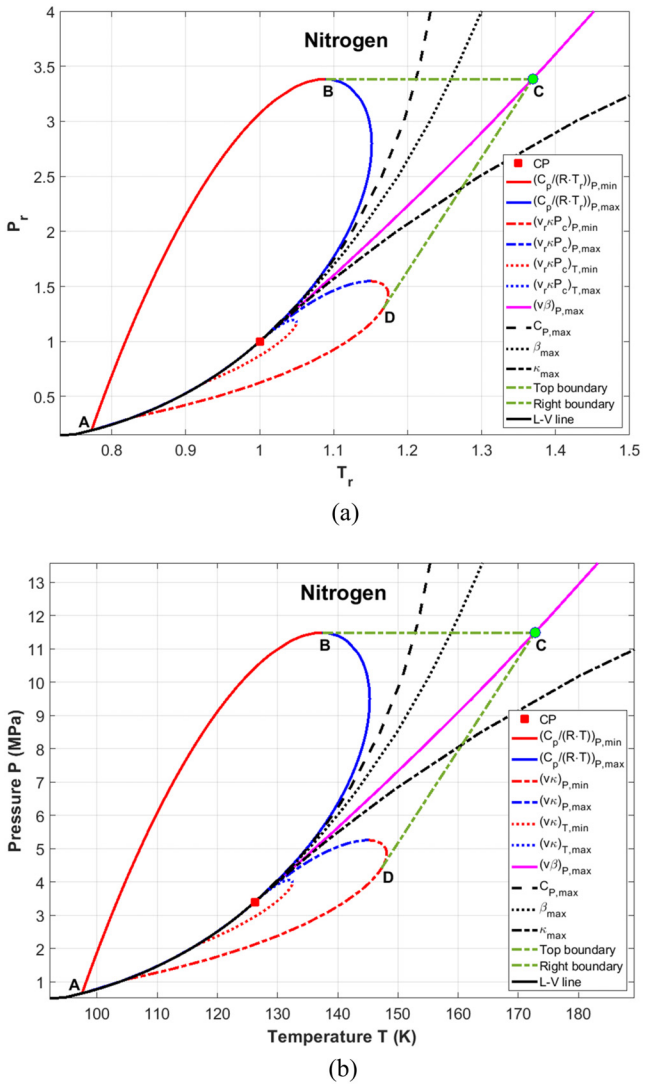

FIG. 15. Closed loops formed by the derivatives of Gibbs free energy for nitrogen: (a) See the caption of Fig. 13(b), closed loops formed by the three third-order functions: $\zeta_{r1} = 0$, $\zeta_{r3} = 0$, and $\zeta_{r4} = 0$. Three Widom lines for $c_{p,max}$, β_{max}, and κ_{max} are superposed on this $P_r - T_r$ map, and (b) replica of (a) in pressure, P (MPa) and temperature, T (K); the values of A–D are given in Table II.

F. Trajectory of liquid–vapor line toward the solid-melt boundary

Finally, we consider the curves of $\zeta_{r2,T} = 0$ in Fig. 19, where the solid lines represent the loci of the maxima while the dotted lines are the loci of the minima. Recall that for the vdW fluid, this line is the same as the critical isochoric line ($v_r = 1$), which starts from the critical point and extends without any bound (Fig. 12). This is an artifact of the vdW EOS, where the isochoric line becomes a straight line in the high-pressure region. As pointed out by Deiters and DeReuck,[43] this is due to the fact that the repulsion term is overestimated and outweighs the attraction term at high pressures in the vdW EOS. Indeed, for the real fluids the lines for (c_p/RT_r) -vs-P exhibit shallow minima in the region of high-pressures, beyond the inflexion points where the maxima end. It is believed that these shallow minima are due to the details of the molecular packing, which may be explained by the statistical thermodynamics of rigid-body fluids.[43]

The reality is that the curves of $\zeta_{r2,T} = 0$ for real fluids do form closed loops, but with the solid/liquid lines (Fig. 19). This is in contrast to the other three loops of minima and maxima (Figs. 13–17). Note that the end of the minima curves meeting the melt/solid lines could

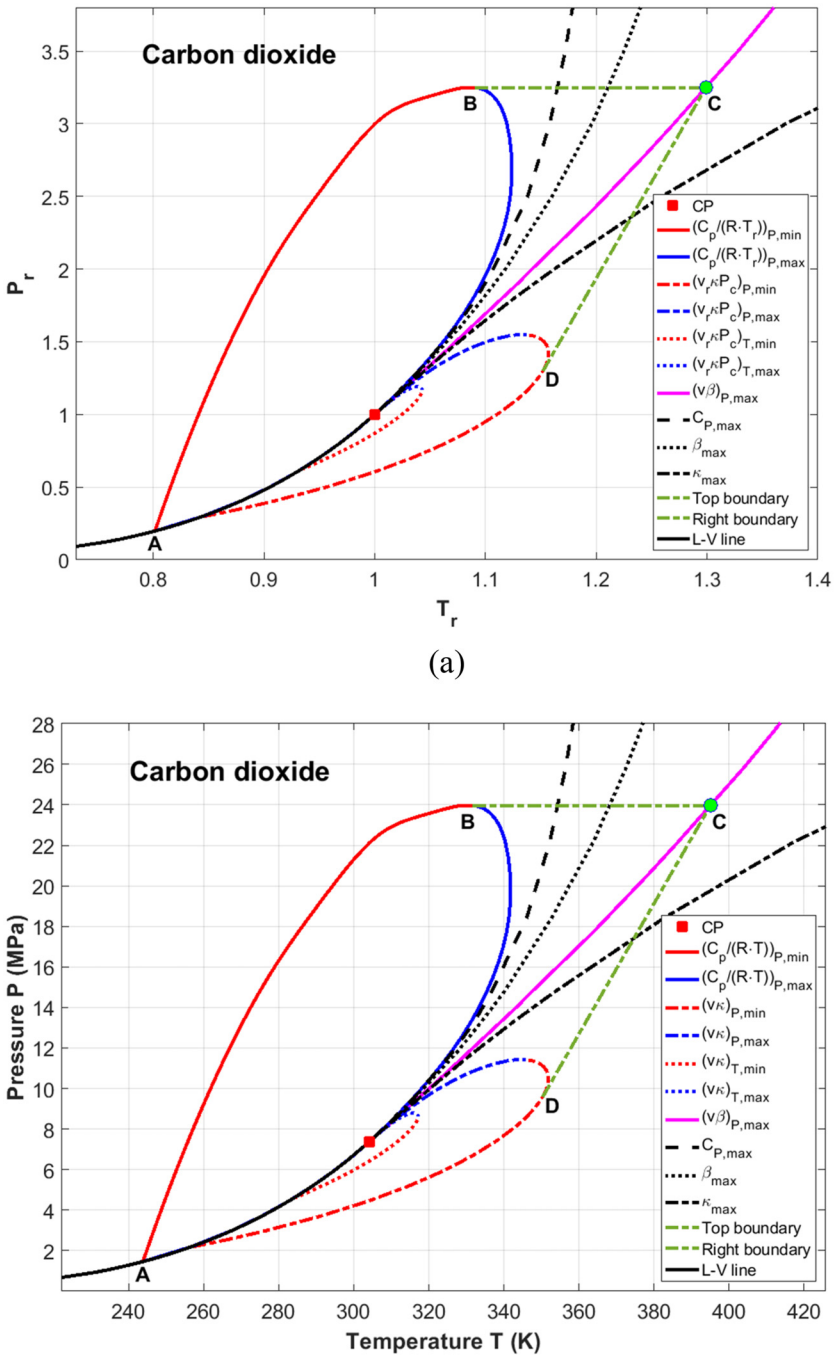

FIG. 16. Closed loops formed by the derivatives of Gibbs free energy for carbon dioxide: (a) closed loops formed by the three third-order functions: $\zeta_{r1} = 0$, $\zeta_{r3} = 0$, and $\zeta_{r4} = 0$. Three Widom lines for $c_{p,max}$, β_{max}, and κ_{max} are superposed on this $P_r - T_r$ map, and (b) replica of (a) in pressure, P (MPa) and temperature, T (K); the values of A–D are given in Table II.

not be shown because the REFPROP[30] does not provide data beyond the pressures and temperatures, as in Fig. 19.

Also, in the case of $\zeta_{r2,T} = 0$, the maxima and minima curves meet at extreme pressures ($P > 20P_c$) and temperatures ($T > 3T_r$) unlike the other three loops, and all of the five curves exhibit similar characteristics (Fig. 19). They emanate from their critical points and move toward high pressures and high temperatures, reaching maximum temperatures, $T_{r,\zeta 2max}$, but with different pressures, $P_{r,\zeta 2max}$. Then, they turn toward lower T_r but higher P_r, finally ending at the solid-liquid line.

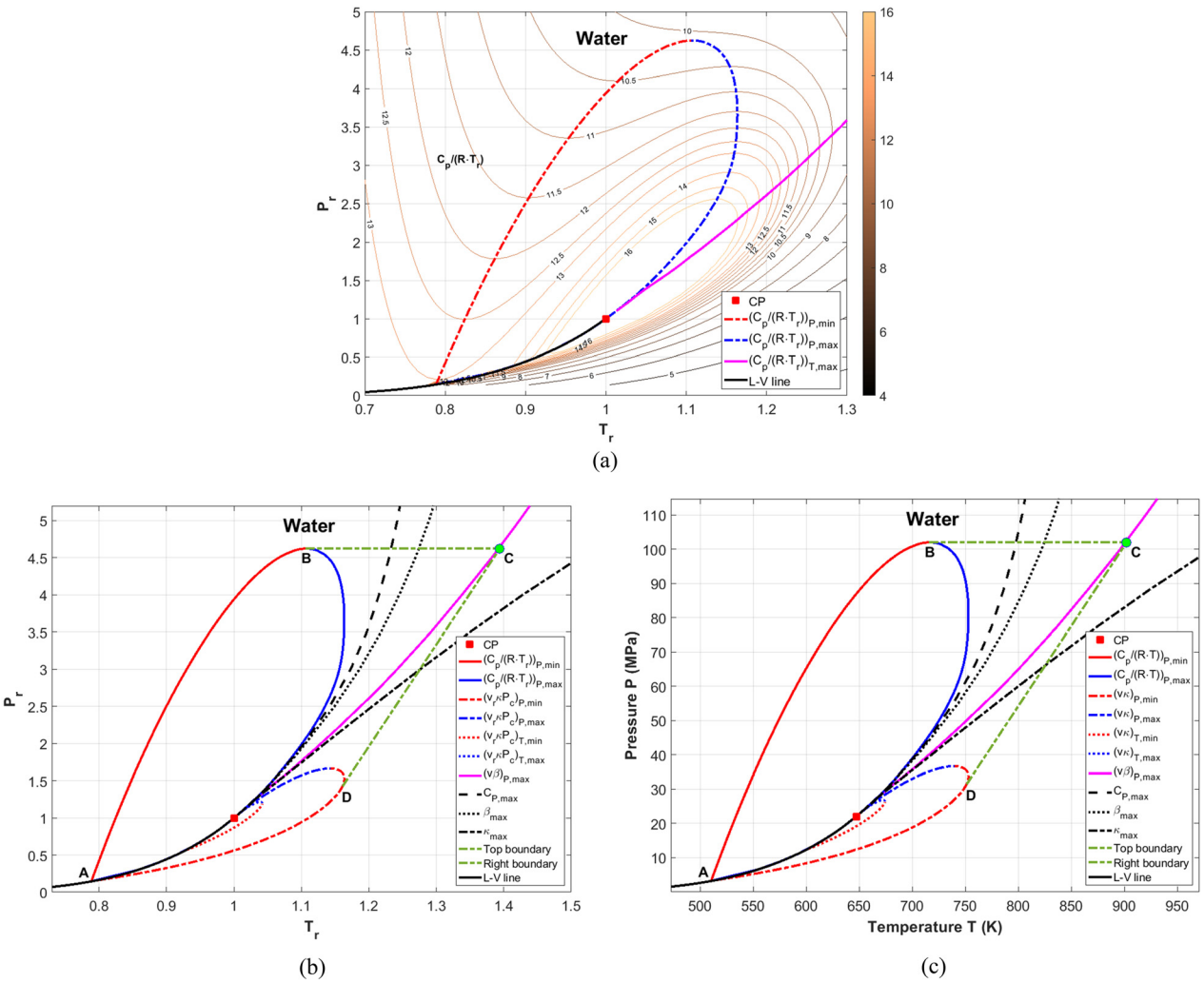

FIG. 17. Closed loops formed by the derivatives of Gibbs free energy for water: (a) contours of c_p/RT_r, superposed are two curves that connect the loci of $\zeta_{r1} = 0$ and $\zeta_{r2} = 0$, representing the extrema of the curves of c_p/RT_r red dashed line for minimum, blue for maximum, and magenta for $(c_p/RT_r)_{T,max}$, and $\zeta_{r2,P} = 0$, and (b) three closed loops formed by $\zeta_{r1} = 0$, $\zeta_{r3} = 0$, and $\zeta_{r4} = 0$ (see Fig. 19 for the loci of $\zeta_{r2,T} = 0$). Three Widom lines for $c_{p,max}$, β_{max}, and κ_{max} are superposed on this $P_r - T_r$ map. The values of A, B, C, and D are given in Table I. (c) replica of (b) in pressure, P (MPa) and temperature, T (K); the numerical values of A–D are given in Table II.

TABLE I. Reduced pressure and temperature of points A–D on Figs. 12, 13(b), 14(a), 15(a), 16(a), and 17(b).

			A		B		C		D	
	ω	Z_c	P_r	T_r	$P_{r,max}$	T_r	P_r	$T_{r,max}$	P_r	T_r
vdw		0.375	0.155	0.664	3.227	1.140	3.227	1.494	1.138	1.172
Ar	−0.002	0.290	0.173	0.730	3.640	1.094	3.640	1.423	1.276	1.167
CH_4	0.011	0.286	0.199	0.768	3.446	1.101	3.446	1.389	1.262	1.164
N_2	0.037	0.289	0.192	0.772	3.383	1.088	3.383	1.379	1.239	1.160
CO_2	0.224	0.274	0.203	0.801	3.252	1.086	3.252	1.299	1.281	1.150
Water	0.344	0.229	0.144	0.788	4.630	1.108	4.630	1.392	1.328	1.154

TABLE II. Numerical values of points A–D on Figs. 13(c), 14(b), 15(b), 16(b), and 17(c).

			A		B		C		D	
	P_c (MPa)	T_c (K)	P (MPa)	T (K)	P_{max} (MPa)	T (K)	P (MPa)	T_{max} (K)	P (MPa)	T (K)
Ar	4.863	150.687	0.841	110.00	17.701	164.85	17.701	214.43	6.205	175.85
CH_4	4.599	190.564	0.915	146.35	15.849	209.81	15.849	264.69	5.804	221.82
N_2	3.396	126.192	0.652	97.42	11.488	137.30	11.488	174.02	4.207	146.38
CO_2	7.377	304.128	1.498	243.61	23.991	330.28	23.991	395.06	9.450	349.75
Water	22.064	647.096	3.177	503.44	102.156	716.98	102.156	900.76	29.301	746.75

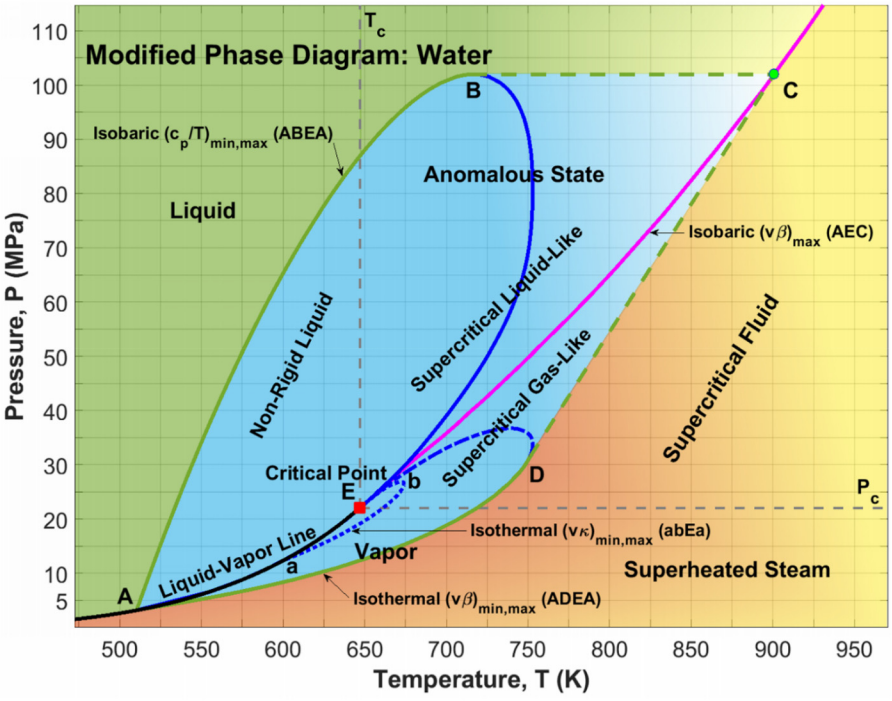

FIG. 18. Proposed modification to the water phase-diagram exhibiting the various phase transitions and the anomalous state. Note that the isobaric $(v\beta)_{max}$ is the same as the isothermal $(c_p/T)_{max}$, and the isothermal $(v\beta)_{max}$ is equal to the isobaric $(v\kappa)_{max}$.

Indeed, the curves of Ar and CH_4 are almost identical for the most part (solid lines for maxima) and deviate slightly in the part of minima (dotted lines). The inflexion points of the two fluids are also close to each other in terms of $T_{r,\zeta 2max}$ and $P_{r,\zeta 2max}$; (3.147, 35.851) for Ar and (3.100, 32.697) for CH_4. This is understandable since both fluids are considered simple fluids with symmetric molecular geometry, a fact that is reflected by their close acentric factors, ω, −0.002 19 for Ar and 0.011 42 for CH_4. However, the curve for N_2 is seen to deviate from these two curves, for example, $T_{r,\zeta 2max}$ and $P_{r,\zeta 2max}$ for N_2 are 2.836 and 33.712, but not too far from that of Ar and CH_4. The acentric factor of N_2 is 0.0372 and N_2 has an asymmetric structure. On the other hand, for CO_2 ($\omega = 0.223\,94$) very different $T_{r,\zeta 2max}$ and $P_{r,\zeta 2max}$ are found, 2.20 and 24.346, respectively. Significant drops in both $T_{r,\zeta 2max}$ and $P_{r,\zeta 2max}$ of CO_2 from N_2, Ar, and CH_4, indicate that $T_{r,\zeta 2max}$ and $P_{r,\zeta 2max}$ are sensitive to the variations in molecular structures of the fluids. In other words, like acentric factor, ω, $T_{r,\zeta 2max}$, and $P_{r,\zeta 2max}$ can also serve as indicators of the fluid structure. Indeed, $T_{r,\zeta 2max}$ and ω correlate very well with each other for these four fluids, which again demonstrates the applicability of the law of corresponding states from the subcritical to supercritical states.

Interestingly, the water (blue line in Fig. 19) follows a similar trend as of the other four fluids in the vicinity of the critical point. However, the behavior changes substantially as the pressure and temperature increase. This can be attributed to the water being a polar fluid that deviates from the nonpolar fluids at high SC pressures and temperature, $P_r > 10$ and $T_r > 2$. Remarkably, the curve suddenly changes its trend with temperature, resulting in a continuous increase in both T_r and P_r. It finally approaches much higher values of $T_{r,\zeta 2max}$ (3.544) and $P_{r,\zeta 2max}$ (85.347), where the inflexion takes place. Beyond the inflexion point, the water curve follows the same trend as others. Evidently, more work is needed to examine the variations at between the polar and non-polar fluids at very high pressures, and also, for how

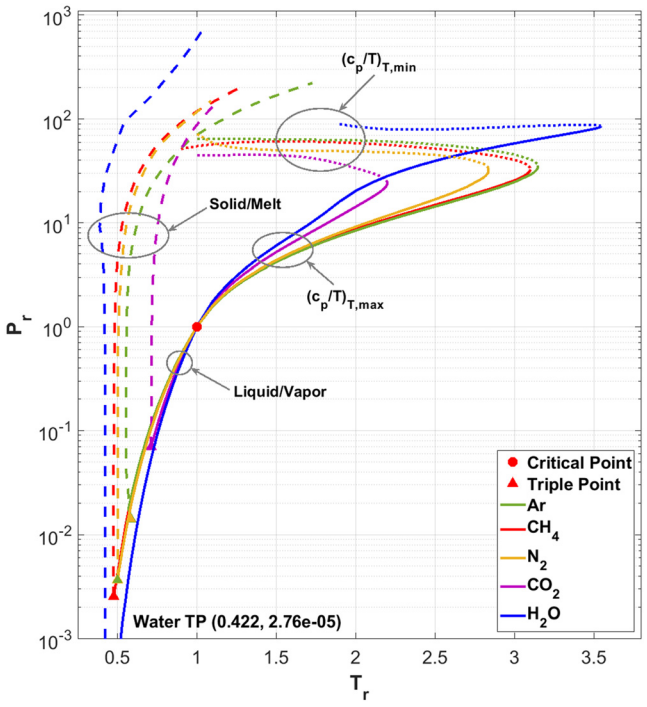

FIG. 19. The loci of $\zeta_{r2,T} = 0$ representing the extrema of the curves of $(c_p/RT_r)_T$; solid lines represent maxima, dotted lines minima which are expected to meet the dashed line representing the solid–liquid melt lines, in each case. (For the vdW fluid, $\zeta_{r2,T} = 0$ line extends infinitely, Fig. 5). The data for melt-solid lines are obtained from Tegeler *et al.*[35] (Ar), Setzmann and Wagner[37] (CH_4), Span *et al.*[36] (N_2), Span and Wagner[38] (CO_2), and Saul and Wagner[44] (water).

the curves for $(c_p/RT_r)_{p,\min}$ ($\zeta_{r2,T} = 0$) meet/merge with the melt-solid lines (Fig. 19).

V. CRITICAL POINT

Historically, the critical point has been defined as the state where the liquid and vapor phases of a fluid become indistinguishable. Essentially, the critical point identifies the end of the liquid–vapor line where the heat (enthalpy) of vaporization becomes zero. Based on the present analysis we can state: "The critical point is a (P, v, T) state, where (a) the anomalies in the fluid properties/behavior are maximal, (b) the third derivative of the Gibbs free energy is zero, and (c) the thermodynamic specific heat, isobaric volumetric expansion, and isothermal compressibility parameters, (c_p/T), $(v\beta)$, and $(v\kappa)$, respectively, approach infinity." In addition, the independent closed loops created by the maxima and minima of these three parameters that identify the anomalous states on the phase diagram, meet at the critical point.

VI. APPLICATION OF THE DELIMITATION OF ANOMALOUS STATE

As Mouahid *et al.*[45] have stated "…the conditions of the pressure and temperature of supercritical processes must be chosen outside these transitory zones. The choice of the best operating conditions depends on the targeted application." Indeed, the delimitation of the anomalous state is critically important to understand the phase transitions from the liquid to SC fluids and its implications to the design and operations of the fluid flow and thermal systems.

1. First, the assumption of liquid being incompressible becomes invalid when the state of the liquid falls in the anomalous region (non-rigid liquid). This is part of the closed loop for (c_p/T), on the left side of the liquid–vapor line in Figs. 12, 13(b), 13(c), 14–16, 17(b), and 17(c). This means the compressibility effects need to be considered in the region right to the red line of $(c_p/T)_{p,\min}$.
2. Since the anomalous region on both the subcritical vapor/gaseous side and the supercritical fluid side, including the Widom Delta as depicted in Figs. 12, 13(b), 13(c), 14(a), 14(b), 15(a), 15(b), 16(a), 16(b), 17(b), and 17(c) can experience large-scale property variations/inversions leading to flow instabilities, thermal oscillations, and/or deteriorated heat transfer. Any system expected to experience this state must be carefully designed and operated. Following are a few scenarios of such possibilities:
   The anomalous region can be looked at in two parts: (A) as temperature, T, increases, the specific heat, c_p increases until it reaches its peak at the critical point, ρc_p shows a similar behavior (Ref. 23), and (B) as T continues to increase further, beyond CP, both c_p and ρc_p may go down. It is then easy to see that in zone A where $(\rho c_p T)$ is continuously increasing, a local thermodynamic inequilibrium can set in if a rapid and sufficient energy transport to the location of this condition cannot take place. Similarly, in zone B a local thermodynamic inequilibrium can occur since with an increase in temperature, c_p is decreased, and the heat may be released. This can further increase the temperature locally, producing an unstable condition if the heat transfer is not rapid. Obviously, these thermal instabilities/oscillations can produce the flow instabilities. In some situations, these changes can be local and of very short durations but in other cases they may be cyclic and can induce long-term or permanent oscillations. In those situations, they are certainly detrimental to the flow and heat transfer systems.
   Furthermore, let us consider the heat transfer to a flowing fluid from a heated surface. If the surface temperature keeps the flow conditions in zone A, the heat transfer will increase since with the increase in the fluid temperature the specific heat, ρc_p would increase. However, if the fluid temperature crosses T_c and moves into the zone B, the heat transfer rate may start decreasing, since ρc_p will decrease, and will go to a lower value. (This deterioration in heat transfer rate, DHT, is not related to the thermal boundary layer thickness.) This DHT can also occur locally, away from the surface, and can create local instability.
3. Since outside the anomalous region on the supercritical side, the properties change monotonically, fluid flow and thermal systems would be stable and no fluctuations/oscillations would be expected. However, the properties will still be strong functions of both pressure and temperature and their variations would need to be accounted for. That means, the effects of volume change, viscous dissipation, compressible (pressure) work, Joule–Thomson cooling, and so on would be quite important under those conditions.

As an example of the applicability of the above, we refer to our recent work, Almara *et al.*[46] that presents safe conditions and gray zones for the transport of SC hydrocarbons and natural gas. Employing the findings in Almara's work, Prasad *et al.*[47] have identified the safe

pressures and temperatures at which supercritical natural gas (SNG) can be transported intercontinentally at very-high-mass flow rates, thousands of kilometers away—without recompression. This distance is much more than that ever achieved or proposed. In addition to demonstrating the benefits of the SNG transport via pipelines at the ocean bottom, they have also analyzed the complex effects of property variations, compressibility, surrounding thermal conditions, Joule–Thomson cooling, and thermal resistance of the pipeline. Interestingly, the pumping power requirement per unit length and per unit mass goes down as the inlet pressure is increased in the SC regime, a huge operational advantage. In the absence of the thermodynamic model presented in this paper, the safe zone was approximated from the plots based on the REFPROP[30] property data. The estimated safe zone for methane, $P > 5$ MPa and $T > 243$ K is quite consistent with Fig. 14(b), the inlet pressure being much higher than 5 MPa and the exit pressure not below 5 MPa. Consequently, Prasad *et al.*[47] have considered the SC pipeline flow of natural gas from the inlet conditions of 30 MPa, 283 K to the exit pressure of 6 MPa. It is evident from Fig. 14(b) that under these conditions, the natural gas consisting of 95% methane will not experience the anomalous behavior during its transit as long as the exit temperature is above 230 K, true to most situations.

The above work[46,47] clearly demonstrates the great potential of high-capacity, long-distance, energy-efficient transport of fluids under SC conditions beyond the anomalous state. In addition, the possibilities of the use of SC heat transfer (working) fluids are enormous. Notable among them are: (a) high-capacity large, medium, and small heat exchangers, (b) energy conversion systems such as the thermal power plants, including nuclear, concentrated solar power, and geothermal/volcanic heat recovery (deep water can be at SC conditions), (c) transport of methane extracted from the methane hydrate buried in the sediments at the ocean bottom (research under progress), (d) high-power heat dissipation in many systems and devices such as the electronics, avionics, server rooms, and data centers, (e) cryogenic cooling, refrigeration, and air conditioning, and (f) space vehicles, satellites, space stations, and lunar systems. Many of these systems will work at SC pressures and temperatures outside the anomalous state whereas many others can be designed specifically to take advantage of the high heat capacity, ρc_p, of SC fluids within the anomalous state; such systems will obviously require precise control of temperature and pressure.

VII. CONCLUSIONS

Major conclusions from this thermodynamic analysis and its application to the vdW fluid, Ar, CH_4, N_2, CO_2, and water, can be summarized as follows:

- Thermodynamically, the most appropriate parameters that govern the anomalous state in the subcritical and supercritical regions are (c_p/T), $(\nu\beta)$, and $(\nu\kappa)$ rather than c_p, β, and κ. They are essentially the second derivatives of the Gibbs free energy and depend on the variation of entropy and specific volume.
- The critical point is the physical state (P, ν, T) where anomalies in the fluid properties/behavior are maximal, the third derivative of the Gibbs free energy is zero, and the thermodynamic parameters (c_p/T), $(\nu\beta)$, and $(\nu\kappa)$ approach infinity.
- The third derivative of the Gibbs free energy as zero, $d^3g = 0$, leads to two extrema (a minimum and a maximum) of these three parameters, (c_p/T), $(\nu\beta)$, and $(\nu\kappa)$, in contrast to c_p, β, and κ which exhibit only maxima, not the minima. The maxima and minima of these parameters form separate closed loops on the P–T phase diagram revealing the regions of strong influence in both the subcritical and supercritical states.
- The first third-order derivative $\zeta_1 = (\partial^3 g/\partial T^3)_P = 0$ leads to the loci of $(c_p/T)_{\mathrm{p,min}}$, and $(c_p/T)_{\mathrm{p,max}}$ and formation of a closed loop. This occurs only in the liquid (subcritical) or liquid-like (supercritical) states and does not cross the liquid–vapor line.
- The second third-order derivative $\zeta_2 = (\partial^3 g/\partial T^2 \partial P) = 0$ yields the demarcation line between the SC liquid-like and gas-like states since it is a natural extension of the liquid–vapor line. For the vdW fluid, this line is the isochoric line of $\nu_r = 1$ and extends without any bounds toward high pressures and high temperatures. However, for the real fluids, the line for $(c_p/T)_{T,\mathrm{max}}$ reaches an inflexion point, turns around, and moves as the $(c_p/T)_{T,\mathrm{min}}$ line toward the melt/solid line, asymptotically. Indeed, the $\zeta_2 = 0$ line presents a unified view of the liquid-to-gas phase transition. Below the critical pressure, liquid-to-gas phase change is the first-order phase transition with distinct changes in all thermodynamic properties, and above CP, it becomes a third-order phase transition with both the specific volume and entropy changing continuously and smoothly.
- The third third-order derivative $\zeta_3 = (\partial^3 g/\partial T \partial P^2) = 0$ represents $(\nu\beta)_{T,\mathrm{min,max}}$ and $(\nu\kappa)_{p,\mathrm{min,max}}$ during an isothermal $(\nu\beta)$ or isobaric $(\nu\kappa)$ expansion (or compression) process. In this region, the trend in the variation of $(\nu\beta)$ with pressure and in $(\nu\kappa)$ with temperature are again in reverse to those outside the region.
- The fourth third-order derivative involves the isothermal derivatives with respect to pressure, $\zeta_4 = (\partial^3 g/\partial P^3)_T = 0$, i.e., the $(\nu\kappa)_{T,\mathrm{min,max}}$ loop. Together with the liquid–vapor line, they enclose a small region near the critical point that represents a new phase and shows an anomalous variation in $(\nu\kappa)$ that is in contrast to the variation of $(\nu\kappa)$ outside this region.
- The above third-order phase transitions as per $(\partial^3 g/\partial T^3)_P = 0$, $(\partial^3 g/\partial T^2 \partial P) = 0$, $(\partial^3 g/\partial T \partial P^2) = 0$, and $(\partial^3 g/\partial P^3)_T = 0$ are related to the ridges discovered and reported in the literature.
- The three Widom lines for $c_{p,\mathrm{max}}$, β_{max}, and κ_{max} fall between the closed loops of $\zeta_1 = (\partial^3 g/\partial T^3)_P = 0$ and $\zeta_3 = (\partial^3 g/\partial T \partial P^2) = 0$, forming the so-called Widom Delta as proposed in the literature.
- The anomalous region can be mapped based on the zeros of the third-order derivatives of the Gibbs free energy. It is considered as the region bounded by the lines for $(c_p/T)_{p,\mathrm{min}}$, $(\nu\beta)_{T,\mathrm{min}}$, the tangent to (c_p/T) loop (the line of $P_{r,\mathrm{max}}$), and the line connecting the $(\nu\beta)_{T,\mathrm{min}}$ curve to the intersection of $P_{r,\mathrm{max}}$ and $\zeta_2 = 0$ line.
- The law of corresponding states is applicable in the anomalous region of non-polar real fluids—Ar, CH_4, N_2, and CO_2, from the subcritical to supercritical states. Water, a polar fluid does show some deviations, particularly in Pr,max.
- The delimitation of the anomalous region is critical to the design and operation of the SC flow and thermal systems as well as to the subcritical systems operating in the vicinity of the liquid–vapor line.

ACKNOWLEDGMENTS

This research has been supported by the U.S. National Science Foundation EAGER via Award No. 2231393 to University of North

Texas (UNT) and Collaborative Research Awards via No. 2327571 to UNT and No. 2327572 to the University of Akron.

AUTHOR DECLARATIONS

Conflict of Interest

The authors have no conflicts to disclose.

Author Contributions

Guo-Xiang Wang: Conceptualization (equal); Formal analysis (equal); Funding acquisition (equal); Investigation (equal); Methodology (equal); Validation (equal); Writing – original draft (equal); Writing – review & editing (equal). **Laura M. Almara:** Data curation (equal); Methodology (equal); Validation (equal); Writing – review & editing (equal). **Vish Prasad:** Conceptualization (equal); Formal analysis (equal); Funding acquisition (equal); Methodology (equal); Writing – original draft (equal); Writing – review & editing (equal).

DATA AVAILABILITY

The data that support the findings of this study are available from the corresponding author upon reasonable request.

NOMENCLATURE

a	Coefficient in van der Waals equation of state
b	Coefficient in van der Waals equation of state
CP	Critical point
c_p	Isobaric specific heat (J kg^{-1} K^{-1})
c_p/T	Isobaric specific heat parameter (J kg^{-1} K^{-2})
EOS	Equation of state
g	Specific Gibbs free energy (J kg^{-1})
h	Specific enthalpy (J kg^{-1})
k	Thermal Conductivity (W m^{-1} K^{-1})
P	Pressure (Pa, MPa)
R	Gas constant (J kg^{-1} K^{-1})
SC	Supercritical
SCGL	Supercritical gas-like
SCLL	Supercritical liquid-like
s	Specific entropy (J kg^{-1} K^{-1})
T	Temperature (°C, K)
v	Specific volume (m^3 kg^{-1})

Greek symbols

β	Isobaric coefficient of volumetric expansion (K^{-1})
κ	Isothermal compressibility (Pa^{-1})
μ	Dynamic viscosity (N s m^{-2})
ρ	Density (kg m^{-3})
ω	Acentric factor
$v\beta$	Isobaric volumetric expansion parameter (m^3 kg^{-1} K^{-1})
$v\kappa$	Isothermal compressibility parameter (m^3 kg^{-1} Pa^{-1})

Subscript

c	Value at critical point
max	At the location of maximum
min	At the location of minimum
p, P	Derivative at constant pressure or an isobaric process
r	Reduced parameter (ratio with respect to the value at CP)
T	Derivative at constant temperature or an isothermal process

Dimensionless parameters

c_p/RT_r	Non-dimensional Isobaric specific heat parameter
$v_r\beta T_c$	Non-dimensional Isobaric volumetric expansion parameter
$v_r\kappa P_c$	Non-dimensional Isothermal compressibility parameter

REFERENCES

[1]A. R. Imre, U. K. Deiters, T. Kraska, and I. Tiselj, "The pseudocritical regions for supercritical water," Nucl. Eng. Des. **252**, 179–183 (2012).
[2]F. Battista, F. Picano, and C. M. Casciola, "Turbulent mixing of a slightly supercritical van der Waals fluid at low-Mach number," Phys. Fluids **26**, 055101 (2014).
[3]D. L. Albernaz, M. D. Quang, J. C. Hermanson, and G. Amberg, "Thermodynamics of a real fluid near the critical point in numerical simulations of isotropic turbulence," Phys. Fluids **28**, 125105 (2016).
[4]W. Yan, X. Jinliang, D. Ming, X. Jian, and W. Qinghua, "Phase distribution in nanochannels of supercritical fluid with different fluid–wall interaction," Phys. Fluids **35**, 062002 (2023).
[5]C. Azih and M. I. Yaras, "Effects of spatial gradients in thermophysical properties on the topology of turbulence in heated channel flow of supercritical fluids," Phys. Fluids **30**, 015108 (2018).
[6]Y. Wang, H. Wang, H. Jin, and L. Guo, "Numerical simulation of adiabatic/cooled/heated spherical particles with Stefan flow in supercritical water," Phys. Fluids **33**, 053305 (2021).
[7]P. Wu, Y. Ren, M. Feng, J. Shan, Y. Huang, and W. Yang, "A review of existing supercritical water reactor concepts, safety analysis codes and safety characteristics," Prog. Nucl. Energy **153**, 104409 (2022).
[8]E. Wang, N. Peng, and M. Zhang, "System design and application of supercritical and transcritical CO_2 power cycles: A review," Front. Energy Res. **9**, 723875 (2021).
[9]S. Shariatnia, A. Asadi, and D. Jarrahbashi, "Experimental analysis of supercritical-assisted atomization," Phys. Fluids **33**, 013314 (2021).
[10]C. Segal and S. A. Polikhov, "Subcritical to supercritical mixing," Phys. Fluids **20**, 052101 (2008).
[11]Y. Li, Z. Li, R. Yang, Y. Zhao, and B. Zhang, "Relationship between physical parameters of supercritical fluids and normal shock characteristics," Phys. Fluids **34**, 116120 (2022).
[12]National Academies of Sciences, Engineering, and Medicine, *Negative Emissions Technologies and Reliable Sequestration: A Research Agenda* (The National Academies Press, Washington, DC, 2019).
[13]K. Nishikawa and T. Morita, "Small-angle x-ray-scattering study of supercritical trifluoromethane," J. Phys. Chem. B **101**, 1413–1418 (1997).
[14]K. Nishikawa and T. Morita, "Inhomogeneity of molecular distribution in supercritical fluids," Chem. Phys. Lett. **316**(3–4) 238–242 (2000).
[15]K. Nishikawa, K. Kusano, A. A. Arai, and T. Morita, "Density fluctuation of a van der Waals fluid in supercritical state," J. Chem. Phys. **118**, 1341–1346 (2003).
[16]K. Nishikawa, A. A. Arai, and T. Morita, "Density fluctuation of supercritical fluids obtained from small-angle x-ray scattering experiment and thermodynamic calculation," J. Supercrit. Fluids **30**, 249–257 (2004).
[17]T. Sato, M. Sugiyama, K. Itoh, K. Mori, T. Fukunaga, M. Misawa, T. Otomo, and S. Takata, "Structural difference between liquidlike and gaslike phases in supercritical fluid," Phys. Rev. E **78**, 051503 (2008).
[18]L. Xu, P. Kumar, P. Buldyrev, S. H. Chen, P. H. Poole, F. Sciortino, and H. E. Stanley, "Relation between the Widom line and the dynamic crossover in systems with a liquid–liquid phase transition," Proc. Natl. Acad. Sci. U. S. A. **102**, 16558–16562 (2005).
[19]G. G. Simeoni, T. Bryk, F. A. Gorelli, M. Krisch, G. Ruocco, M. Santoro, and T. Scopigno, "The Widom line as the crossover between liquid-like and gas-like behaviour in supercritical fluids," Nat. Phys. **6**, 503–507 (2010).

[20]V. V. Brazhkin, Y. D. Fomin, A. G. Lyapin, V. N. Ryzhov, and E. N. Tsiok, "Widom line for the liquid–gas transition in Lennard–Jones system," J. Phys. Chem. B **115**, 14112–14115 (2011).
[21]Y. D. Fomin, V. N. Ryzhov, E. N. Tsiok, V. V. Brazhkin, and K. Trachenko, "Thermodynamics and Widom lines in supercritical carbon dioxide," arXiv:1411.6849 [Cond-mat.stat-mech] (2014).
[22]A. R. Imre, A. Groniewsky, G. Györke, A. Katona, and D. Velmovszki, "Anomalous properties of some fluids—with high relevance in energy engineering—in their pseudo-critical (Widom) region," Period. Polytech., Chem. Eng. **63**(2), 276–285 (2019).
[23]V. Prasad, K. Kakroo, and D. Banerjee, "Existence of supercritical 'liquid-like' state in subcritical region, optimal heat transfer enhancement, and argon as a non-reacting, non-corroding SC heat transfer fluid," Heat Transfer Res. **53**(9), 1–27 (2022).
[24]V. V. Brazhkin, Y. D. Fomin, A. G. Lyapin, V. N. Ryzhov, and K. Trachenko, "Two liquid states of matter: A dynamic line on a phase diagram," Phys. Rev. E **85**, 031203 (2012).
[25]D. T. Banuti, M. Rajub, and M. Ihme, "Between supercritical liquids and gases—Reconciling dynamic and thermodynamic state transition," J. Supercrit. Fluids **165**, 104895 (2020).
[26]M. Y. Ha, T. J. Yoon, T. Tlusty, Y. Jho, and W. B. Lee, "Widom delta of supercritical gas−liquid coexistence," J. Phys. Chem. Lett. **9**, 1734–1738 (2018).
[27]T. J. Yoon, M. Y. Ha, W. B. Lee, and Y. W. Lee, "Probabilistic characterization of the Widom delta in supercritical region," J. Chem. Phys. **149**, 014502 (2018).
[28]D. T. Banuti, "Crossing the Widom-line—Supercritical pseudo-boiling," J. Supercrit. Fluids **98**, 12–16 (2015).
[29]C. Cockrell, V. V. Brazhkin, and K. Trachenko, "Transitions in super-states of matter," Phys. Rep. **941**, 1–27 (2021).
[30]E. W. Lemmon, I. H. Bell, M. L. Huber, and M. O. McLinden, *NIST Standard Reference Database 23: Reference Fluid Thermodynamic and Transport Properties-REFPROP, Version 10.0* (NIST, 2018).
[31]F. A. Gorelli, T. Bryk, M. Krisch, G. Ruocco, M. Santoro, and T. Scopigno, "Dynamics and thermodynamics beyond critical point," Sci. Rep. **3**, 1203 (2013).
[32]A. Bejan, *Advanced Engineering Thermodynamics*, 4th ed. (Wiley, 2016).
[33]D. T. Banuti, M. Raju, and M. Ihme, "Similarity law for Widom lines and coexistence lines," Phys. Rev. E **95**, 052120 (2017).
[34]D. C. Johnston, *Advances in Thermodynamics of the Van Der Waals Fluid* (Morgan & Claypool Publishers, San Rafael, 2014).
[35]C. Tegeler, R. Span, and W. Wagner, "A new equation of state for argon covering the fluid region for temperatures from the melting line to 700 K at pressures up to 1000 MPa," J. Phys. Chem. Ref. Data **28**, 779–850 (1999).
[36]R. Span, E. W. Lemmon, R. T, Jacobsen, W. Wagner, and A. Yokozeki, "A reference equation of state for the thermodynamic properties of nitrogen for temperatures from 63.151 to 1000 K and pressures to 2200 MPa," J. Phys. Chem. Ref. Data **29**, 1361–1433 (2000).
[37]U. Setzmann and W. Wagner, "A new equation of state and tables of thermodynamic properties for methane covering the range from the melting line to 625 K at pressures up to 1000 MPa," J. Phys. Chem. Ref. Data **20**, 1061–1155 (1991).
[38]R. Span and W. Wagner, "A new equation of state for carbon dioxide covering the fluid region from the triple-point temperature to 1100 K at pressures up to 800 MPa," J. Phys. Chem. Ref. Data **25**, 1509–1596 (1996).
[39]W. Wagner and A. Pruss, "The IAPWS formulation 1995 for the thermodynamic properties of ordinary water substance for general and scientific use," J. Phys. Chem. Ref. Data **31**, 387–535 (2002).
[40]P. Gallo, D. Corradini, and M. Rovere, "Widom line and dynamical crossovers as routes to understand supercritical water," Nat. Commun. **5**, 5806 (2014).
[41]W. Wagner and A. Kruse, *The Industrial Standard IAPWS-IF97 for the Thermodynamic Properties and Supplementary Equations for Other Properties, - Properties of Water and Steam* (Springer Verlag, Heidelberg, 1997).
[42]E. N. de Jesús, J. Torres-Arenas, and A. L. Benavides, "Widom line of real substances," J. Mol. Liq. **322**, 114529 (2021).
[43]U. K. Deiters and K. M. DeReuck, "Guidelines for publication of equations of state—I. Pure fluids: Technical report," Chem. Eng. J. **69**(1), 69–81 (1998).
[44]A. Saul and W. Wagner, "A fundamental equation for water covering the range from the melting line to 1273 K at pressures up to 25000 MPa," J. Phys. Chem. Ref. Data **18**, 1537–1564 (1989).
[45]A. Mouahid, P. Boivin, S. Diaw, and E. Bidens, "Widom and extreme lines as criteria for optimizing condition in supercritical processes," J. Supercrit. Fluids **186**, 105587 (2022).
[46]L. M. Almara, G. X. Wang, and V. Prasad, "Conditions and thermophysical properties for transport of hydrocarbons and natural gas at high pressures: Dense phase and anomalous supercritical states," J. Gas Sci. Eng. **117**, 205072 (2023).
[47]V. Prasad, L. M. Almara, and G. X. Wang, "Ultra-long-distance transport of supercritical natural gas (SNG) at high-mass flow rates via pipelines through land, underground, water bodies, and ocean," J. Gas Sci. Eng. **117**, 205053 (2023).